Advances in Water Resources 125 (2019) 13–31

Contents lists available at ScienceDirect

Advances in Water Resources

journal homepage: www.elsevier.com/locate/advwatres

Streamflow, stomata, and soil pits: Sources of inference for complex models with fast, robust uncertainty quantification

M. Chase Dwelle[a], Jongho Kim[a,b], Khachik Sargsyan[c], Valeriy Y. Ivanov[a,*]

[a] Department of Civil and Environmental Engineering, University of Michigan, United States
[b] School of Civil and Environmental Engineering, University of Ulsan, Ulsan, South Korea
[c] Sandia National Laboratories, Livermore, CA 94550, United States

ARTICLE INFO

Keywords:
Ecohydrology
Hydrologic modeling
Uncertainty quantification
Sensitivity
Parameter inference
Bayesian compressive sensing

ABSTRACT

The scale and complexity of environmental and earth systems introduce an array of uncertainties that need to be systematically addressed. In numerical modeling, the ever-increasing complexity of representation of these systems confounds our ability to resolve relevant uncertainties. Specifically, the numerical representation of the governing processes involve many inputs and parameters that have been traditionally treated as deterministic. Considering them as uncertain introduces a large computational burden, stemming from the requirement of a prohibitive number of model simulations. Furthermore, within hydrology, most catchments are sparsely monitored, and there are limited, heterogeneous types of data available to confirm the model's behavior. Here we present a blueprint of a general approach to uncertainty quantification for complex hydrologic models, taking advantage of recent methodological developments. We rely on polynomial chaos machinery to construct accurate surrogates that can be efficiently sampled for the ecohydrologic model tRIBS-VEGGIE to mimic its behavior with respect to a selected set of quantities of interest. The use of the Bayesian compressive sensing technique allows for fewer evaluations of the computationally expensive tRIBS-VEGGIE. The approach enables inference of model parameters using a set of observed hydrologic quantities including stream discharge, water table depth, evapotranspiration, and soil moisture from the Asu experimental catchment near Manaus, Brazil. The results demonstrate the flexibility of the framework for hydrologic inference in watersheds with sparse, irregular observations of varying accuracy. Significant computational savings imply that problems of greater computational complexity and dimension can be addressed using accurate, computationally cheap surrogates for complex hydrologic models. This will ultimately yield probabilistic representation of model behavior, robust parameter inference, and sensitivity analysis without the need for greater investment in computational resources.

1. Introduction

In research areas of physical hydrology and ecohydrology, computational models are used to improve the understanding and predictions of watershed and ecosystem dynamics. Recent developments towards these objectives include modeling at higher resolutions and investigating sensitivities of hydrologic response to watershed properties and climate forcings (e.g., Getirana et al., 2014; Guan et al., 2015; Kim and Ivanov, 2015; Krakauer et al., 2014; Ringeval et al., 2014; Rudorff et al., 2014). Likewise, in climate assessment studies, resolving complex systems and associated feedbacks requires the representation of relevant dynamics at commensurate spatial and temporal scales (Abril et al., 2014; Brown and Lugo, 1982; Cramer et al., 2004; Detwiler and Hall, 1988). Tackling this complexity calls for models that rely on details of mechanistic interactions and therefore demand large computational resources to provide more robust assessments and predictions (Bisht et al., 2017).

Estimates from computational models are affected by a number of uncertainty sources that can be partitioned into reducible and irreducible uncertainties (Beven, 2013; Beven et al., 2016; De Rocquigny, 2012). These uncertainties can be amplified due to the complexity and nonlinearity of addressed problems. Therefore it is prudent to apply a formal uncertainty quantification (UQ) machinery to evaluate them. More broadly, one needs a holistic approach to UQ to seamlessly encapsulate *all* uncertainties of computer simulations within their specific contexts. This is a valuable pursuit for many computational sciences, not just hydrology, and as such, UQ has emerged in the last two decades as an active research field, which has incorporated applied mathematics, engineering, and physical sciences (e.g., Ghanem and Doostan, 2006; Gilbert et al., 2016; Knio and Le Maître, 2006; Najm, 2009; Sargsyan et al., 2014; Xiu and Tartakovsky, 2004).

The overarching goal of UQ is to provide improvements in predictions and understanding of key sources and magnitudes of uncertainty,

* Corresponding author.
E-mail address: ivanov@umich.edu (V.Y. Ivanov).

https://doi.org/10.1016/j.advwatres.2019.01.002
Received 18 August 2018; Received in revised form 8 December 2018; Accepted 6 January 2019
Available online 9 January 2019
0309-1708/

which can inform decision making and control for management of natural and engineered systems (Ascough Ii et al., 2008; da Cruz et al., 1999; García et al., 2015; Morss et al., 2005). The quantification of uncertainties related to a prediction of a physical system involves two associated problems: (1) the estimation of model input variables (e.g., parameterization constants, input forcings), addressed by comparing model simulations with available observational data or data products (i.e., synthesized data and model estimates), and (2) the forward propagation of uncertainty from input variables to output quantities of interest (QoIs).

Quantifying uncertainties has long been a goal in hydrologic modeling (Beven, 1993; Beven and Westerberg, 2011; Renard et al., 2010). Inference of input parameters is common (e.g., Abbaspour et al., 2004; McLaughlin and Townley, 1996; Vrugt et al., 2008), however, robust quantification of uncertainties for complex models remains an area of acute interest (Beven et al., 2015; Chen et al., 2011; Hall et al., 2014; Krzysztofowicz, 2001). Firstly, traditional UQ methods carry computational burden that makes working with models of higher complexity difficult. Secondly, simpler, lumped models in hydrology cannot provide information on variables that originate from physically rich solutions; they therefore cannot take the full advantage of heterogeneous (in terms of space-time coverage or target variables) observational data sets that are typical of sparsely monitored watersheds. Many UQ studies have used conceptual rainfall runoff models (e.g., Renard et al., 2010; Vrugt et al., 2008) that permit fast computation and use of variations of Markov Chain Monte Carlo (MCMC) sampling (Gilks et al., 1995; Hastings, 1970) for UQ. Complex, integrated models of hydrology (e.g., Kollet et al., 2017; Maxwell et al., 2014), however, require much greater computational resources making the (tens of thousands of) simulations required via MCMC analysis computationally prohibitive. An approach to reduce this computational burden is to construct a *surrogate* or *metamodel* to approximate the behavior of the complex hydrologic model (e.g., Elsheikh et al., 2014; Razavi et al., 2012).

Recent advancements in UQ applications have examples of comprehensive, fully integrated surface and subsurface flow models (Gilbert et al., 2016; Miller et al., 2018). The methodologies used in these studies still required hundreds of simulations in order to accomplish rigorous uncertainty assessments. In the case where wall-clock simulation time for a larger-scale watershed is considerable (e.g., days to weeks), more efficient methods are required.

This study offers an approach with a UQ framework applied to a quasi-three-dimensional hydrologic model with surface and variably-saturated subsurface flows, as well as vegetation biophysics that resolves energy budgets. This framework allows the likelihood-based estimation of input parameters using a diverse set of observations. To display the abilities of the framework in a setting of real-world challenges, the study domain is a small, sparsely monitored tropical catchment in the Amazon rainforest.

Previously, large-scale studies of the Amazon have been undertaken to understand the importance of how hydrology and carbon cycles interact (e.g., Fan and Miguez-Macho, 2010; Lin et al., 2015; Miguez-Macho and Fan, 2012a; Miguez-Macho and Fan, 2012b; Pokhrel et al., 2013). Many of these studies have simulated the entire Amazon region, using grid cell discretization of $\mathcal{O}(10\,[\mathrm{km}])$ (e.g., Beighley et al., 2009; Coe et al., 2008; Yamazaki et al., 2011, or somewhat finer (Miguez-Macho and Fan, 2012a; 2012b). However, as has been previously shown (e.g., Miguez-Macho and Fan, 2012b), this discretization does not resolve the basic functional hydrologic units — hillslopes and, as a result, the lateral mass fluxes from higher-elevation areas to the valleys of the drainage network. Ignoring the connection between upstream recharge areas and downstream discharge regions can have important consequences on robustness of studies that depend on understanding space-time variability of the hydrologic regime (Kim et al., 1999; Salvucci and Entekhabi, 1995). Important ecohydrologic processes occur in these upstream, lower-order, headwater catchments (Richey et al., 2011; 2009). Vital, smaller scale studies of these upland areas have been undertaken (e.g., Cuartas et al., 2012; Fang et al., 2017; Fleischbein et al., 2006; Nobre et al., 2011), but no thorough uncertainty assessments were performed. Limited sensitivity experiments performed carried out in Fang et al. (2017), Vertessy and Elsenbeer (1999) were applied to these catchments, however a sufficiently general framework of uncertainty quantification and sensitivity analysis of hydrologic response of watersheds with scarce data is still absent in the literature.

The objective of this study is to demonstrate a novel approach to the representation and propagation of model input uncertainties by implementing what has been termed non-intrusive spectral projection Le Maître and Knio (2010) to construct a surrogate model to emulate the behavior of a complex hydrologic model. This methodology allows us to model, at high spatial resolutions, the ecohydrologic interaction between groundwater and surface water in a small upland catchment in Amazonia. It also permits a general approach to account for uncertainties in model parameters and initial conditions of the groundwater surface. Specifically, this work focuses on quantifying uncertainty in the soil parameterizations of the Asu research catchment (e.g., Cuartas et al., 2012; Tomasella et al., 2008), focusing on the challenge of probabilistic estimates of bulk soil properties in this sparsely-monitored watershed.

In the methodology section, we introduce (i) the mechanistic model for this study: tRIBS-VEGGIE (TIN-based Real-time Integrated Basin Simulator—Vegetation Generator for Interactive Evolution), (ii) construction of a surrogate model for tRIBS-VEGGIE through polynomial chaos expansions (PCEs), (iii) dimensionality reduction methods to more efficiently construct the PCE surrogate model, and (iv) accelerated inference of tRIBS-VEGGIE model parameterizations using PCE surrogates. The case study of the Asu watershed demonstrates the construction of a surrogate model representation and sensitivity analysis carried out with it. This representation is then used to perform parametric inference, highlighting the flexibility of the framework to identify uncertainties and use diverse observational data for parameter estimation. The parameters obtained from inference are then used to compute hydrologic output from tRIBS-VEGGIE. The benefits and limitations of this framework are addressed in the end, with a focus on issues in hydrologic modeling that benefit from an uncertainty quantification approach.

2. Methods and study design

This study provides a framework to derive uncertain model parameters for a sparsely gauged catchment using a physically rich model tRIBS-VEGGIE and its simplified mathematical representation, i.e., a surrogate model. The sparse availability of groundwater, soil properties, and streamflow data in the watershed is recognized and accounted for in the designs so that different data types can be used to inform the model's behavior. This section describes the data available in the catchment and reports an approach for dealing with the lack of observational data available within the modeling and uncertainty quantification framework.

2.1. Simulation setup

The watershed domain is located approximately 76 [km] northwest of Manaus, Brazil (Fig. 1a). The watershed is part of activities carried under the Large-Scale Biosphere-Atmosphere (LBA) Experiment in Amazonia managed by the National Institute of Amazonian Research (INPA). This location was chosen due to the long record of available atmospheric forcing data from a flux tower installed in 1999 as well as the availability of relevant data from streamflow gauges, soil moisture sensors, and groundwater piezometers. This catchment is one of the most instrumented catchments in the Amazon Basin, surrounded by undisturbed rainforest. This region is characterized by a tropical monsoonal climate, with average annual rainfall of approximately 2400 [mm], average annual temperature of 26 °C, and a wet season from November–May and dry season from June–October (Cuartas et al., 2007; 2012; Nobre et al., 2011).

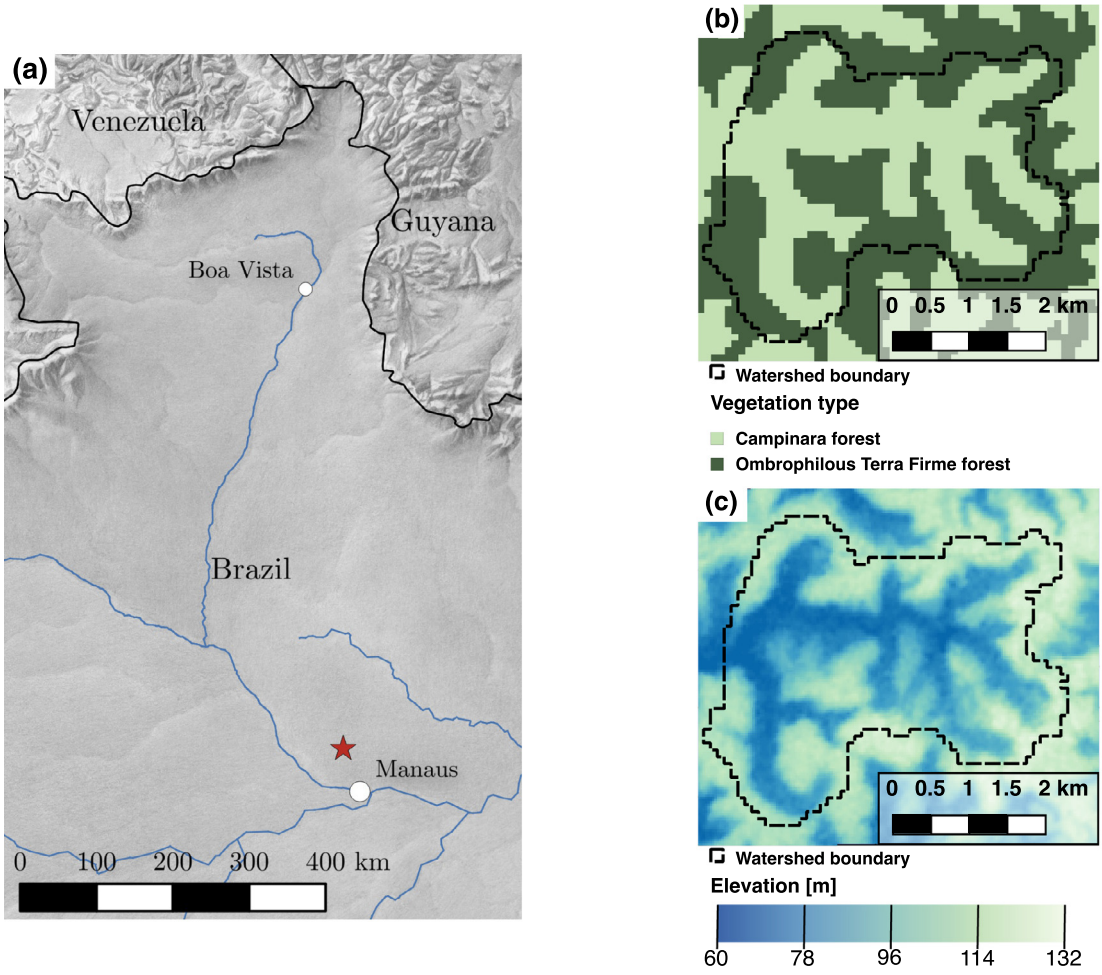

Fig. 1. The study location, labeled by the red star in (a), is approximately 76 [km] N-NW of Manaus, Brazil. Manaus lies at the confluence of the Negro and Solimões rivers, and at this confluence the Amazon River begins. The vegetation types for the Asu watershed are shown in (b) as derived in Cuartas et al. (2012). The spatial distribution of elevation within the watershed is illustrated in (c).

2.1.1. Representation of simulation domain

The simulation domain, the Asu watershed (Fig. 1b, c), represents a zero- to third-order basin in Amazonia, previously detailed in (Cuartas et al., 2007; 2012; Nobre et al., 2011). The total area is 12.4 [km^2], and the watershed has varying soil thickness, with a maximum between 40 and 50 [m] (Cuartas et al., 2012). To represent its subsurface domain, the layer thickness is fixed at 40 [m] using 35 irregularly resolved mesh layers, increasing from 0.04 [m] for the surface layer, to 2.5 [m] for the layers between 5 and 40 [m]. The thickness of the layers increase following a geometric series such that, as the soil depth increases, each layer is some fraction r thicker than the previous layer: $\Delta z_{i+1} = \Delta z_i(1+r)$, up to the depth $z_i = 5$ [m]. For this domain we chose $r = 0.296$, which allows for smaller soil layers near the surface, and larger layers towards the bottom of the soil domain. This discretization enables the capture of the dynamics of infiltration and lateral water movement in the vadose zone, while maintaining computational efficiency. In the horizontal plane, the domain is represented using 3 arc-second (90×90 [m]) spacing from the SRTM digital elevation model (Jarvis et al., 2008), resulting in 1554 square Voronoi cells. Overall, this gives $1,554 \times 35 = 54,390$ computational nodes in the domain.

2.1.2. Soil type and land cover

Previous classification of soils for this site have been undertaken in (Cuartas et al., 2012; Fang et al., 2017; Tomasella et al., 2008), but focused on the near-surface soil properties at few locations that are hard to interpret in terms of their changes with depth (see also Fang et al., 2017). The detailed soil classification such as the one given in Cuartas et al. (2012) can be useful, but understanding effective, watershed-scale properties (i.e., that represent the catchment as a whole) is frequently of more relevance, since the vast majority of basins are ungauged and have little to no data on soil properties. In the context of a sparsely gauged watershed, it can also be useful to know how changes in model parameterizations within the watershed affect the simulation results of important hydrologic variables such as streamflow, water table depth, evapotranspiration, etc. Recently, Fang et al. (2017) also used a bulk soil properties case instead of the finer detailed properties available in Cuartas et al. (2012). Consequently, while in no way required by the applied UQ framework (Section 2.3), this study assumes that there is a single soil type in the watershed, whose effective physical characteristics need to be estimated inversely. We represent soil properties with a high degree of uncertainty, taking into account the full ranges of soil property values used in previous studies (Cuartas et al., 2012; Fang et al., 2017).

Specifically, the uncertain parameterizations used for soil properties are calculated using the pedotransfer function for Brazilian soils from Tomasella et al. (2000). This study used multivariate linear regression relying on texture (percentages of sand, silt, and clay), organic carbon, moisture equivalent, and bulk density to fit a second-order polynomial for the dependent variables of α, n, θ_r and θ_s of the van Genuchten soil water retention and model (van Genuchten, 1980). Furthermore, the study of Broedel et al. (2017) provides data on texture and bulk density

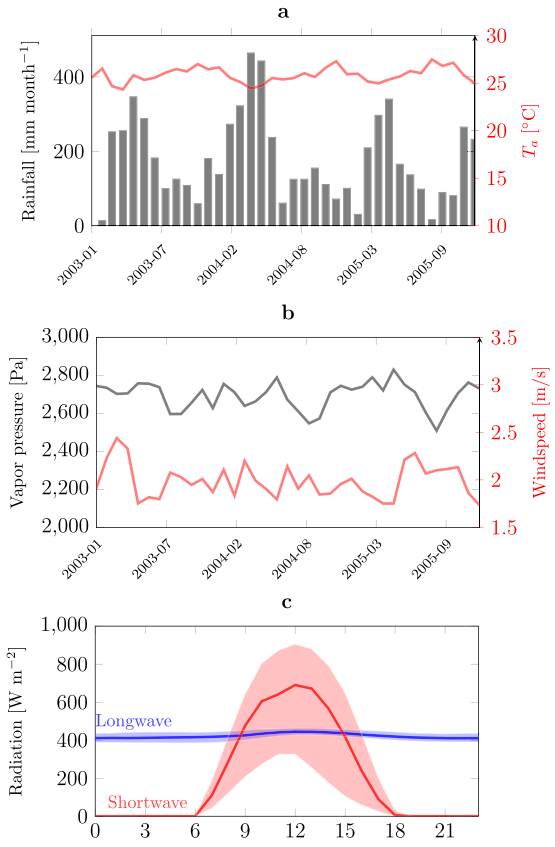

Fig. 2. Atmospheric forcings used in simulations. (**a**): Monthly aggregated rainfall (grey bars) and air temperature (red line). (**b**) Monthly averaged vapor pressure and wind speed. (**c**): The diurnal cycle of longwave and shortwave radiation estimated for the entire simulation period. The line of each represents the median, and the shading is between the 10- and 90-percent quantiles.

for the Asu catchment up to a depth of 14.3 [m], and the estimate for moisture equivalent is given in Tomasella et al. (2000).

The two classes of vegetation present in the catchment are (a) *terra firme* forest on the plateau and sloped areas, and (b) *Campinarana* forest (Ranzani, 1980) in the valleys and ecotone areas of the watershed (Fig. 1b). The Type (a) forest has dense evergreen tropical vegetation with heights of approximately 30 [m]. The Type (b) forest is less dense with tree heights typically around 20–25 [m] (Cuartas et al., 2012). The parameterizations for these vegetation types followed (Cuartas et al., 2012).

2.1.3. Climate forcing

Climate forcing data are available at hourly intervals for 26,300 [h] from January 1, 2003 to January 1, 2006. The region exhibits wet and dry seasons spanning from approximately November–May and June–October, respectively. Aggregated time series of data used for forcing the model are shown in Fig. 2 (Restrepo-Coupe et al., 2013). These data are spatially uniform across the watershed.

2.1.4. Initial and boundary conditions

For solving subsurface flow dynamics, the flux (Neumann) boundary condition was specified at the surface (net rainfall) and bottom (zero flux) of the domain, allowing for infiltration, runoff, and exfiltration fluxes. For surface flow, an open boundary (in the form of free outfall) was assumed at the downstream end (Kim et al., 2016a). The watershed was delineated from the downstream end, therefore for all other boundaries of the watershed, the no-flux (solid slip wall) boundary condition was specified.

2.1.5. Quantities of interest

Within uncertainty quantification, a quantity of interest (QoI) is an output from a numerical model whose response to uncertain inputs is evaluated. Each QoI needs to be a scalar, but many QoIs can be considered such that one can examine temporal or spatial responses. In practice thousands of QoIs can be defined, such as a time series of the model's output, or a single QoI may be selected if it is believed to carry significant information about the phenomenon being studied (e.g., the mean water table depth). For this study, a mix of targeted quantities of interest is selected to include domain-aggregated quantities of interest and time series of both domain-aggregated and point-location QoIs, which are provided in Table 1. These QoIs include: daily and monthly streamflow, daily streamflow in the 95th percentile, mean monthly soil water content in the top 1 [m], evapotranspiration, mean monthly evapotranspiration, and depth to water table for six wells or group of wells. The data available in the watershed means that some QoIs can be used to infer model parameters (Section 2.4). Those QoIs that coincide with observations are used for parameter estimation (denoted in the "Inference" column of Table 1), and those that are not are only used for estimation.

The number of scalars belonging to each group of QoIs is given in the fourth column of the Table 1, with a total of 499 QoIs for this study. Those QoIs used in inference were constrained to periods where data were available, e.g., the soil moisture data in the study area only exist for January-October of 2005 (see Fig. 4) at a single soil pit location adjacent to the flux tower at the study site (Restrepo-Coupe et al., 2013). Therefore, the construction of a time series of monthly mean soil water content leads to ten QoIs. Although these soil moisture data are only representative of the hydrologic behavior in the upland area near the flux tower, it can still be included as a quantity of interest and used in inference. Outlet streamflow was collected starting December 2004 and running through December 2005, however these data were only sampled once daily, often with several days, or sometimes periods of weeks between sampling. Due to the absence of continuous observed streamflow, monthly aggregated mean streamflow was used as a QoI to construct the surrogate model.

Water table data in the watershed were sampled between 2012–2015, outside the time period for this study. Additionally, they were sampled at irregular periods with days or weeks between readings. While twelve well locations were sampled, not each location was sampled during both the wet and dry season, and several wells were in close proximity to each other. Due to these issues, wells that had at least ten recordings in both the wet and dry seasons were kept for analysis. After exclusion, the remaining ten wells were aggregated into groups based on their location within computational cells in tRIBS-VEGGIE, i.e., if two or more well locations were in the same computational cell of 90 [m] × 90 [m], the data from these locations were combined into a group for analysis. After this aggregation, six well groups remained with water table depths between 0.5 and 5 [m] (Fig. 4).

Even in the absence of data representative of the entire spatial and temporal domain of the study, all (i.e., any) available data can be included for analysis with the UQ framework. Their inclusion provides data for inference (Section 2.4). A strength in this approach is that one is not constrained to a single hydrologic process or specific data type (such as the time series or mean quantities) when performing inference. Any data available that can be represented in the hydrologic model are suitable for use with the UQ machinery outlined in Section 2.3.

In Table 1, the distinction for the "dry" period for $\mathcal{TS}(ET_{\text{dry}})$ refers to a month exhibiting a cumulative water deficit (CWD):

$$CWD_i = \begin{cases} \sum_{j=1}^{D} P_j - ET_j & \text{if } \sum_{j=1}^{D} P_j - ET_j < 0 \\ 0 & \text{if } \sum_{j=1}^{D} P_j - ET_j > 0 \end{cases}, \tag{1}$$

where P_j and ET_j are the daily accumulated daily precipitation and evapotranspiration, respectively, where j denotes the day in month i. The time period for all reported QoIs are the year 2005, and during this period there was a negative CWD in August, September, and October of 2005 of −49.1, −80.6, and −87.5 [mm], respectively.

Table 1
Quantities of interest selected for this study. Those denoted $\mathcal{TS}(\cdot)$ are time series of a specific QoI. The "Inference" column denotes whether that QoI was used in inference of model parameters in Section 3.2, and N is the number of surrogates constructed for each QoI.

QoI	Description	Inference	N
$\mathcal{TS}(Q)$	Daily time series of streamflow [$m^3\ s^{-1}$]		365
$\mathcal{TS}(Q_{\text{month}})$	Monthly aggregated streamflow [$m^3\ s^{-1}$]	Y	13
$Q_{0.95}$	Daily streamflows in the 95th percentile [$m^3\ s^{-1}$]		1
$\mathcal{TS}(\theta_{\text{1m}})$	Mean monthly soil water content in top 1 [m] [$mm^3\ mm^{-3}$]	Y	10
$\mathcal{TS}(ET_{\text{dry}})$	Evapotranspiration in dry periods [mm day^{-1}]		92
$\mathcal{TS}(ET_{\text{month}})$	Mean monthly evapotranspiration [mm day^{-1}]	Y	12
WT	Depth to water table [m]	Y	6

Table 2
Uncertain soil parameters $\boldsymbol{X}$ used in the workflow of Fig. 3. The fraction of coarse and fine sand (F_{CS}, F_{FS}), required for the pedotransfer function in Tomasella et al. (2000), is determined based on the sampled values of F_C and F_S, such that $F_{CS} = \alpha_{cs}(1 - F_C - F_S)$ and $F_{FS} = (1 - \alpha_{cs})(1 - F_C - F_S)$. $U[A, B]$ denotes the uniform distribution with support $[A, B]$. The anisotropy ration (a_r) is defined for soil hydraulic conductivities and assumed uniform for the entire range of wetness conditions.

Parameter	Description	Distribution
F_C	Fraction of clay [%]	U[45, 65]
F_S	Fraction of silt [%]	U[15, 25]
α_{cs}	Fraction of sand that is coarse [%]	U[45, 55]
M_e	Moisture equivalent [g g^{-1}]	U[0.1, 0.25]
ρ_b	Bulk density [g cm^{-1}]	U[1.1, 1.2]
k_s	Saturated hydraulic conductivity [mm h^{-1}]	U[2.0, 30]
a_r	Horizontal:vertical anisotropy ratio [-]	U[1, 2]

To construct computationally efficient, surrogate model representations for each QoI, one generates a set of training and validation samples from the uncertain parameters $\boldsymbol{X}$ in Table 2. Each parameter X_i is scaled to a standard uniform variable for computational input, $\xi_i \in [-1, 1]$. These are then run in a set of training simulations through $\mathcal{M}$ to construct the computationally efficient surrogate as detailed in Section 2.3.1. Finally, the performance of the surrogate is evaluated using the set of validation simulations.

2.2. Hydrologic model

The representation of the hydrologic response of a tropical catchment strongly depends on reliable modeling of subsurface flows. tRIBS-VEGGIE (Ivanov et al., 2008; 2010) emulates essential processes of water and energy dynamics over the complex topography of a river basin. Each computational element has a canopy layer that contains two "big-leaves" (sunlit and shaded) representing the canopy. Above-ground processes are coupled to a multi-layer soil model that computes soil moisture, root water uptake, and heat transport using the one-dimensional Richards equation (Hillel, 1980) and the heat diffusion equation, in the direction normal to the element's surface. Gravity-driven flow for the unsaturated lateral exchange is assumed and the Dupuit–Forchheimer approximation (Bear, 1979) for the saturated lateral exchange is implemented. Subsurface flows are routed using the D-∞ flow routing algorithm (Tarboton, 1997), and the flow directions change dynamically for the saturated zone, leading to spatial dynamics that reproduce the three-dimensional numerical solutions (Hopp et al., 2015). In this study, vegetation dynamics are not simulated. Only the biochemical model of photosynthesis and canopy stomatal behavior (Collatz et al., 1991; Farquhar et al., 1980; Leuning, 1990; 1995) is used to simulate the response of latent heat flux to above- and below-ground conditions. The amount

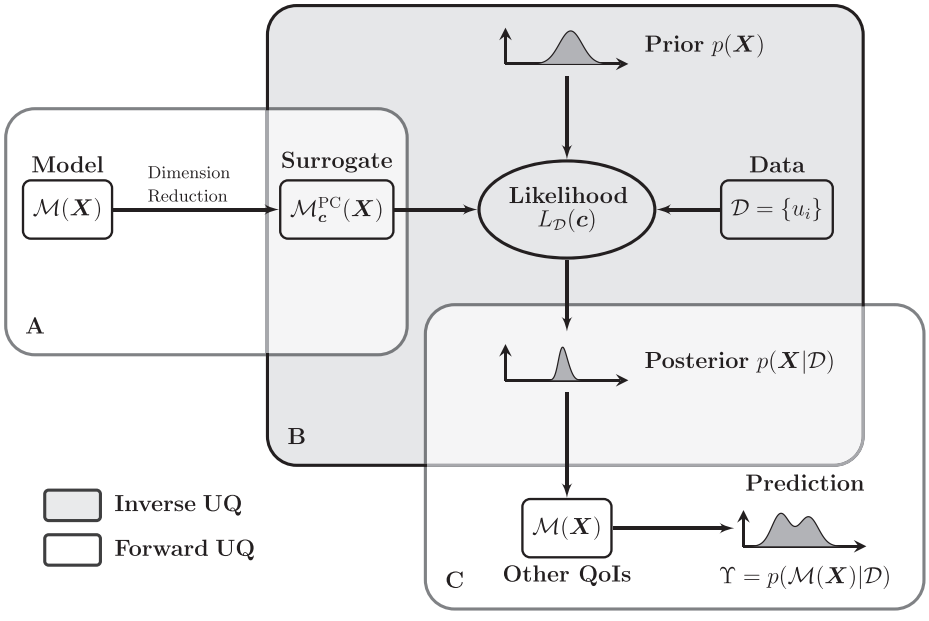

Fig. 3. An overview of an uncertainty quantification (UQ) workflow. The set of methods in each box can be carried out on its own, or used within the general UQ implementation scope illustrated here. In the "Forward UQ" boxes, uncertain inputs ($\boldsymbol{X}$ or $p(\boldsymbol{X} \mid D)$) are propagated through a model. The processes "Dimension Reduction" and "Likelihood" are in ellipses, which represents that there is a modeling decision to be made on the structure of the surrogate model and likelihood function, respectively. Box (A) is the process of constructing a polynomial surrogate of the hydrologic model. Box (B) describes how hydrologic data D are used to perform inverse inference on a set of model parameters $\boldsymbol{X}$ to obtain the parameter posterior distribution $p(\boldsymbol{X} \mid D)$. The resultant posterior distribution can be used in a set of procedures in box (C) that propagate uncertainty propagation in the original model $\mathcal{M}$ (or $\mathcal{M}^{\text{PC}}$) in order to get probabilistic estimates of QoIs.

of leaf area as well as other structural characteristics of vegetation are imposed as pre-determined model input (see Section 2.1.1).

2.2.1. Selection of uncertain inputs

One source for hydrologic uncertainties in the Amazon is the presence of deep soils which give rise to fluctuating groundwater across climes and seasons (Cuartas et al., 2012; Miguez-Macho and Fan, 2012b). Due to difficulties in instrumenting and measuring groundwater, data are sparse: and even experimental catchments have few wells drilled for measuring water table depth. The spatial distribution and initial states of groundwater can impact hydrologic models, such as spin up performance of the model (e.g., Ajami et al., 2014; Seck et al., 2015) or providing better estimates of the impacts on below-surface processes to earth system models (Clark et al., 2015; Riley et al., 2011). Additionally, accurate representation of groundwater processes at smaller scales can provide valuable information to larger scale groundwater processes and their impacts on earth system processes (Fan, 2015; Fan et al., 2013; Krakauer et al., 2014; Riley and Shen, 2014).

The large soil column depths in the Amazon mean that the parameterizations of soil properties in a hydrologic model may have a large effect on the simulated groundwater and vadose zone dynamics. Some field or lab measurements may exist for the soil properties through core testing or well pump tests, but these are limited to accessible areas and may not necessarily represent bulk soil properties in the catchment (Kowalsky et al., 2004; Russo and Bouton, 1992).

In this study, soil parameterizations are selected as uncertain inputs into tRIBS-VEGGIE. The soil properties that represent the uncertain model parameters $\boldsymbol{X}$ are treated as random variables with distributions provided in Table 2. To represent uncertainty in the soil water retention curve characteristics of the soil, the parameters for the pedotransfer function (F_C, F_S, α_{CS}, M_e, ρ_b—see Section 2.1.2) are treated as uncertain. Values for the saturated conductivity (k_s) and the anisotropy ratio (a_r) were not a part of this pedotransfer function, but represent the infiltration and lateral transport characteristics of the soil. These are therefore also treated as uncertain with value ranges estimated using the studies of Cuartas et al. (2012) and Fang et al. (2017).

2.2.2. Water table initializations given soil parameter uncertainty

Given that the soil parameterizations are treated as uncertain, water table initializations that adequately represent the initial state of the water table within the watershed are required. For example, a shallow water table will result under a simulation with a soil type with a low hydraulic conductivity, and a deeper water table will result with a higher hydraulic conductivity. Setting the water table to some fixed value for the entire basin, then allowing steady flow conditions to develop for a given soil type through forcing and draining requires computational resources (e.g., Seck et al., 2015), which would be a detriment to the desired efficiency from the UQ approach in this paper. Groundwater well data for the watershed (e.g., Cuartas et al., 2012; Fang et al., 2017) are available only for a few locations along a transect in the watershed. This limitation, in both spatial and topographic spaces (e.g., elevation, height above nearest drainage, slope, etc.) implies that the available data are inadequate to create meaningful realizations of initial depth to water table to be used in simulations. However, groundwater plays an important role in seasonal flooding and ET dynamics of the Amazon (Miguez-Macho and Fan, 2012a; 2012b). It must be accounted for in any comprehensive hydrologic modeling and therefore some uncertainty should be associated with the water table initialization.

In this work, uncertainty in the initial depth to water table is propagated through parametric uncertainty using a subset of the uncertain parameters in Table 2. Specifically, the initial water table depth is estimated using an adapted mapping function from Sivapalan et al. (1987). This method supposes that there is a steady state groundwater profile throughout the basin and that the streamflow at initialization time $Q(t = 0)$ is derived from a constant, spatially uniform recharge to the groundwater. Furthermore, each location in the basin has a contribution q_i defined by its position in the watershed drainage network:

$$q_i = \frac{a_c Q}{A}, \tag{2}$$

where q_i is the saturated lateral flow, a_c is the surface contributing area of a computational cell, Q is the semi-steady state discharge at the basin outlet, and A is the total basin area. This approach also assumes that the water table is parallel to the soil surface, so the subsurface drainage aligns with the topographical gradient. The water table depth for a single computational cell is given by:

$$N_{\text{iwt}} = -\frac{1}{f} \ln \left[\frac{f a_c Q}{A K_0 a_r W \tan S_0} \right], \tag{3}$$

where N_{iwt} is the initial local water table depth, K_0 is the surface saturated hydraulic conductivity, f is the exponential decay parameter of K_0 with depth (Beven, 1982), a_r is the soil anisotropy ratio (Ivanov et al., 2004), W is the width of the saturated flow between cells, and S_0 is the surface slope.

The decay parameter f is not used in the representation of the soil hydraulic model in this work. However, the rest of the parameters of Eq. (3) are known and therefore a value of f can be solved for a given set of soil parameters and local watershed characteristics at any location. Specifically, the water table depths N_{iwt} are derived by taking the temporal average of water table depths for each observation location described in Section 2.1.5; the values of K_0 and a_r are treated as uncertain and obtained from sampling (see Table 2); and the rest of the variables in Eq. (3) are derived from the basin topography. This leaves f as the only unknown of the equation and therefore, f can be derived for each soil type in the UQ framework through least squares optimization to fit the data to the model in Eq. (3). The estimated value of f for each soil type used in the UQ procedure enables the generation of an initial spatial distribution of water table, specific to the soil parameterization used in the simulation.

The initial water table fields generated through this process were checked for their consistency and magnitudes, with the mean and variability in the initial water table fields given in Fig. S1. The use of the outlined approach provides a realistic representation of the water table depth and also offers an initialization tuned to the uncertain soil parameters.

2.3. Uncertainty quantification framework

tRIBS-VEGGIE has a large set of inputs that could be treated as uncertain; these are closures for certain approximations to physical laws or parameters describing a property of a medium, for example, important for the movement of water in the domain (e.g., saturated conductivity for different soil types present in the domain). In addition to these parameters, there are input fields that describe spatial or temporal states of the simulation watershed. These parameters and fields represent the assumptions made about the makeup and behavior of the domain. They are inherently uncertain since it is not possible to have perfect information about the system being modeled, and this is especially true for natural systems. Therefore, instead of encoding assumptions into single estimates about the system in question, we embrace the uncertainty in our knowledge and attempt to quantify the consequences of this uncertainty on simulation results. In this study, only parametric inputs to tRIBS-VEGGIE will be treated as uncertain to focus on the application of the UQ methodology, with a discussion of the use of spatial input fields for UQ in Section 4,

2.3.1. Surrogate modeling

Let's consider a model $\mathcal{M}$ (i.e., tRIBS-VEGGIE in this study) with inputs $\mathbf{x}$, where $\mathbf{x} = \{x_1, x_2, \ldots, x_M\}$ (e.g., $M = 7$ for this study). This model is used to predict some output quantity of interest (QoI) $\hat{y} \in \mathbb{R}$, where $\hat{y}$ can be assumed to be a scalar quantity for now, but it can (and will) be used for multiple QoIs in this work. This model can be viewed

as a simple function that maps uncertain inputs to an uncertain output:

$$\hat{y} = \mathcal{M}(\mathbf{x}). \tag{4}$$

We assume that $\mathcal{M}$ is a *deterministic* model that can scale in complexity depending on the problem being solved (e.g., in its simplest form it could be $\mathcal{M}(\mathbf{x}) = \sum x_i$). Where uncertainty quantification becomes interesting is when $\mathcal{M}$ is complex, such as the numerical solutions to the governing equations of fluid flow. It is not uncommon for investigations of fluid flow to make single evaluations of the model represented by Eq. (4) and treat it as a "black box," i.e., the internal model dynamics are assumed unknown and only a relationship between model inputs and outputs is analyzed. The only requirement that is imposed on the model is that it must be executable, i.e., provided its inputs $\mathbf{x}$, the model produces its output $\hat{y}$.

If we believe that the model $\mathcal{M}$ adequately captures the dynamics of the system being modeled, then we can also believe that the output $\hat{y} = \mathcal{M}(\mathbf{x})$ we receive from the model gives an accurate prediction, when the values of the input parameters/variables $\mathbf{x}$ are known. However, a typical case for the majority of models of environmental systems is that input values are uncertain, either due to natural variability in the system (e.g., Kim et al., 2016b; Kim et al., 2016c) or inadequate knowledge of parameter values, in general. In this case, it is appropriate to represent these input parameters as uncertain, so they follow a random vector

$$\boldsymbol{X} \sim \pi(\mathbf{x}), \tag{5}$$

where $\boldsymbol{X} = (X_1, X_2, \dots, X_M)$ and $\pi(\mathbf{x})$ is a vector of marginal (and therefore independent) probability density functions (PDF) describing the variability in each of the M uncertain variables in $\boldsymbol{X}$, which are known and defined prior to modeling. Random input variables to the model result in QoIs that can also be treated as a random, i.e.:

$$Y = \mathcal{M}(\boldsymbol{X}). \tag{6}$$

With uncertainty propagation, we are interested in determining the probability distribution of Y. For example, if Y roughly follows a Gaussian distribution, the mean and variance of Y could be considered as estimates of the location and scale of the distribution. However, with complex interactions occurring within the model $\mathcal{M}$, the distribution of Y could be multi-modal or have large skewness or kurtosis, making conventional methods relying on the assumption of Gaussian behavior a poor approximation. As an illustration, consider that if the model output of interest has a similar variability as the prediction quantity Y in Fig. 3, one cannot describe the output distribution through its first moments, and the full characterization of the density function is required.

In order to investigate uncertainties and sensitivities of model outputs to its inputs, many model runs must be performed. This has traditionally been done using collocation methods — taking a sample from the input distribution and identifying the output value resulting from that sample — allowing for the construction of a probability density function of the model's outputs. This is often done using Monte Carlo methods, but the computational expense of Monte Carlo methods quickly scales with the complexity of the model and is prohibitive when multivariate problems are considered (Blatman and Sudret, 2011; Marzouk and Xiu, 2009). An alternative approach is to approximate the fully deterministic model with a polynomial expansion used to create a *surrogate* model (also known as *metamodel*) (e.g., Miller et al., 2018; Najm, 2009; Ricciuto et al., 2018; Xiu and Tartakovsky, 2004). The approach of metamodeling is used to offset the cost of forward, computationally expensive deterministic simulations by approximating the latter with inexpensive surrogate models. *Polynomial chaos expansions* (PCEs) represent one such metamodeling technique that provides an approximation to a computer model through its spectral representation on a basis of polynomial functions (Elsheikh et al., 2014; Najm, 2009).

Specifically, if we have a set of relationships as described in Eqs. (4)–(6), we wish to approximate the deterministic model $\mathcal{M}$ with a suitable polynomial expansion. The expansion relies on polynomial basis terms $\Psi_m(\boldsymbol{X})$ that are orthogonal with respect to the distribution of $\boldsymbol{X}$, meaning $\int_{-\infty}^{\infty} \Psi_m(\mathbf{x})\Psi_n(\mathbf{x})\pi(\mathbf{x})\,\mathrm{d}\mathbf{x} = 0$ for all $m \neq n$, where m and n denote indices of a polynomial sequence and the integral represents the inner product of polynomials with a weighting function $\pi(\boldsymbol{x})$. The model output can then be approximated with (Le Maître and Knio, 2010; Xiu and Karniadakis, 2002):

$$Y = \mathcal{M}(\boldsymbol{X}) \approx \sum_{\boldsymbol{\alpha} \in \mathbb{N}^M} c_{\alpha} \Psi_{\alpha}(\boldsymbol{X}). \tag{7}$$

The uncertain input $\boldsymbol{X}$ will have an associated polynomial $\Psi_{\boldsymbol{\alpha}}$, where $\boldsymbol{\alpha} = (\alpha_1, \alpha_2, \dots, \alpha_M)$ is a multi-index introduced to simplify notation and represents the ordering of terms in the polynomial. An illustration of the multi-index and how it leads to the construction of a PCE is included in the Supplementary Materials S.2.

One typically models the *stochastic* dimension M to be equal to the number of uncertain variables $\boldsymbol{X} = \{X_1, \dots, X_M\}$. The parameters $\{c_{\alpha}\}$ are deterministic polynomial expansion coefficients, and $\{\Psi_{\alpha}(\boldsymbol{X})\}$ are multivariate polynomials orthogonal with respect to the random variables $\boldsymbol{X}$. The multivariate polynomials $\{\Psi_{\alpha}(\boldsymbol{X})\}$ in Eq. (7) are defined as products of univariate polynomials (Le Maître and Knio, 2010, App. C):

$$\Psi_{\alpha}(\boldsymbol{X}) = \prod_{i=1}^{M} \Psi_{i,\alpha_i}(X_i). \tag{8}$$

Based on the marginal distributions of random variables in $\boldsymbol{X}$, different polynomial bases are used Xiu and Karniadakis (2002). Examples of continuous orthogonal polynomials are provided in Table S1. The property of orthogonality implies that the first two moments of uncertain quantity of interest Y can be extracted analytically from the expansion coefficients $c_{\boldsymbol{\alpha}}$, enabling very efficient moment evaluation. See S.2 for an example.

In practice, the right hand side of Eq. (7) is a finite sum through a truncated PCE (Lin and Karniadakis, 2009; Xiu and Karniadakis, 2002):

$$Y = \mathcal{M}(\boldsymbol{X}) \approx \mathcal{M}^{\mathrm{PC}}(\boldsymbol{X}) = \sum_{j=0}^{P} c_j \Psi_j(\boldsymbol{X}), \tag{9}$$

where j is a count of the multiindices α with a predefined order; this is discussed further in the Supplementary Materials. There are a number $P+1$ polynomial basis functions. A typical truncation rule, a total degree truncation of degree p, i.e. $\sum_{i=1}^{M} \alpha_i \leq p$ leads to (see Xiu and Karniadakis, 2002):

$$P + 1 = \frac{(M+p)!}{M!\,p!}, \tag{10}$$

We select a finite number of terms by only including those with a total degree of polynomials from Eq. (8) smaller than a certain value p. Once the selection of uncertain input variables and the polynomial basis (Table S1) has been made, one can solve the polynomial chaos expansion (Eq. (9)) non-intrusively, meaning that the pre- and post-processing of model inputs and outputs takes place without having to make any changes to the mechanistic model $\mathcal{M}$. To do this, one treats the fully deterministic model $\mathcal{M}$ as a heuristic/black-box model to inform the metamodel $\mathcal{M}^{\mathrm{PC}}$ constructed through the polynomial chaos expansion.

The goal is to obtain the right hand side of Eq. (9), where c_j are deterministic weighting coefficients, and Ψ_j are the polynomial expansions of the order associated with the index j for realized (sampled) values of $\boldsymbol{X}$. The values for the coefficients $\mathbf{c} = \{c_0, c_1, \dots, c_P\}$ allow the calculation of the distribution of model output Y as it was induced from the model input $\boldsymbol{X}$. These coefficients are calculated by solving Eq. (9) through either Gaussian quadrature (Smolyak, 1963), regression (Berveiller et al., 2006; Blatman and Sudret, 2008; 2011; Tibshirani, 1996), or Bayesian approaches (Doostan and Owhadi, 2011; Sargsyan et al., 2014). The next step is to estimate the distribution of model output Y as informed by the uncertain (but pre-defined through marginal PDFs) model input $\boldsymbol{X}$. The approximate response of Y is obtained through sampling, often Markov-Chain Monte Carlo (MCMC) (Haario et al., 2001), because the constructed surrogate model in Eq. (9) is much cheaper computationally

than a complex original deterministic model $\mathcal{M}$. The surrogate model $\mathcal{M}^{\mathrm{PC}}$ is assessed using samples of the random vector $\boldsymbol{X}$. These samples can be taken via, e.g., random uniform, stratified, or Latin hypercube sampling (McKay et al., 1979), where the latter is used in this work.

The above considerations result in the feasibility of calculating a polynomial chaos expansion of the model response by using Monte-Carlo or other sampling techniques (Eldred and Burkardt, 2009; Marzouk and Xiu, 2009). In addition to the convenience of numerical approximation, the first two moments of the model output are obtained from the coefficients of the constructed PCE such that the mean μ and variance σ^2 of a scalar model output can be calculated as in Le Maître and Knio (2010):

$$\mu^{PC} = \mathbb{E}\left[\mathcal{M}^{PC}(\boldsymbol{X})\right] = c_0 \tag{11}$$

$$(\sigma^2)^{PC} = \mathrm{Var}\left[\mathcal{M}^{PC}(\boldsymbol{X})\right] = \mathbb{E}\left[\left(\mathcal{M}^{PC}(\boldsymbol{X}) - \mu^{PC}\right)^2\right] = \sum_{j=1}^{P} c_j^2. \tag{12}$$

The previous section was undertaken with a single QoI Y. For multiple QoIs $\boldsymbol{Y} = \{Y_i\}, i = 1, \ldots, K$, the preceding process is carried out for each QoI, i.e., each QoI is a scalar-valued output of $\mathcal{M}$ which can be represented by a surrogate. The remainder of the methodology assumes a single QoI unless otherwise noted.

2.3.2. Bayesian compressive sensing for PCE construction

The limiting factor in the surrogate modeling approach to uncertainty quantification is the amount of model simulations one can perform with the expensive deterministic model $\mathcal{M}$ in order to solve for the coefficients in Eq. (9). There may be a large number M of uncertain variables X to address in the model, which may result in the "curse of dimensionality" (Caflisch, 1998; Davis and Rabinowitz, 2007), i.e., it is not feasible to adequately sample the high-dimensional input variables to construct the surrogate model $\mathcal{M}^{\mathrm{PC}}(\boldsymbol{X})$. Techniques that have been used to address this issue include sparse regression techniques (e.g., Blatman and Sudret, 2008; Blatman and Sudret, 2011; Vidaurre et al., 2013) and the Bayesian compressive sensing (BCS) approach for the PC framework introduced by Sargsyan et al. (2014).

Bayesian compressive sensing (BCS) (Ji et al., 2008; Sargsyan et al., 2014) aims to identify a sparse set of the coefficients c_j to satisfy Eq. (9). This is in contrast to other truncation methods used for PCEs such as total degree, tensor product, or hyperbolic cross (see Sargsyan et al., 2014), which treat each dimension (input variable) equally, or truncate the expansion *a priori*. One would like to select a basis set containing terms that convey *meaningful* contributions to model output Y, while discarding terms that do not. For example, if one chooses uncertain input variables that do not have a dependence relation to each other in the hydrologic QoI, then one would expect basis terms that account for the interaction of these variables to be zero. Including these terms provides no further information or variance in the hydrologic process of interest. With this motivation, this study uses Bayesian compressive sensing (BCS) (Babacan et al., 2010; Ji et al., 2008; Sargsyan et al., 2014) to find a sparse set of coefficients to satisfy Eq. (9). Details of this approach are left to Sargsyan et al. (2014) with a brief overview provided in Appendix A.

The practical implications of employing the BCS technique is that it can greatly reduce the size of the basis set required to construct the surrogate model. Therefore, the technique limits the impact of the "curse of dimensionality" stemming from treating a large number of parameters as uncertain. The amount of this reduction is problem and model dependent, but generally grows relative with the number of uncertain input variables, due to the number of higher-order interaction terms that arise. For example, a problem with 20 uncertain model parameters will have a larger percentage reduction in required simulations of the model $\mathcal{M}$ than a problem with five uncertain parameters.

2.3.3. Sensitivity analysis

Once the surrogate model (9) has been constructed, the use of Monte Carlo methods allows the computation of Sobol' indices for global sensitivity analysis of the model to its input uncertain variables (Saltelli, 2002; Sobol, 2001; Sudret, 2008). In the context of PCE surrogate models, estimates of Sobol' indices is gained directly from the PC surrogate, offering a convenient and computationally efficient way to determine the relative importance of uncertain inputs to the variability of the quantities of interest. Sobol' indices are split into *main* and *joint* sensitivities, where the former measures the fraction of variance in the output that can be attributed to the uncertain model input variable X_i:

$$S_i = \frac{\mathrm{Var}\left[\mathbb{E}\left[\mathcal{M}_{\mathbf{c}}^{\mathrm{PC}}(\boldsymbol{X}) \mid X_i\right]\right]}{\mathrm{Var}\left[\mathcal{M}_{\mathbf{c}}^{\mathrm{PC}}(\boldsymbol{X})\right]}, \tag{13}$$

where $\mathbb{E}$ and Var are operators for expectation and variance, respectively. Similarly, the joint sensitivity measures the fraction of variance in the output that can be explained by to the joint contribution of variables X_i and X_j, and is defined as

$$S_{ij} = \frac{\mathrm{Var}\left[\mathbb{E}\left[\mathcal{M}_{\mathbf{c}}^{\mathrm{PC}}(\boldsymbol{X}) \mid X_i, X_j\right]\right]}{\mathrm{Var}\left[\mathcal{M}_{\mathbf{c}}^{\mathrm{PC}}(\boldsymbol{X})\right]} - S_i - S_j. \tag{14}$$

An additional benefit of using PCE machinery for the surrogate model is that the Sobol' sensitivities in Equations (13) and (14) can be calculated directly from the coefficients of the PCE using the relations from Eqs. (11) and (12), one can write the main and joint Sobol' indices in terms of the PCE coefficients. This yields an estimate for the main effect index $\hat{S}_i^{\mathrm{main}}$ as:

$$\hat{S}_i^{\mathrm{main}} = \frac{\sum_{\boldsymbol{\alpha} \in \mathcal{A}_i^{\mathrm{main}}} c_{\boldsymbol{\alpha}}^2 \left\langle \Psi_{\boldsymbol{\alpha}}^2 \right\rangle}{\sum_{\boldsymbol{\alpha} \in \mathcal{A}, \boldsymbol{\alpha} \neq 0} c_{\boldsymbol{\alpha}}^2 \left\langle \Psi_{\boldsymbol{\alpha}}^2 \right\rangle}, \tag{15}$$

where $\mathcal{A}_i^{\mathrm{main}} = \left\{\boldsymbol{\alpha} \in \mathrm{A} : \alpha_i > 0, \alpha_{i \neq j} = 0\right\}$. Similarly, one can use the PCE coefficients to account for the variance contribution between interactions of X_i and X_j through the estimate of the total effect index $\hat{S}_i^{\mathrm{total}}$:

$$\hat{S}_i^{\mathrm{total}} = \frac{\sum_{\boldsymbol{\alpha} \in \mathcal{A}_i^{\mathrm{total}}} c_{\boldsymbol{\alpha}}^2 \left\langle \Psi_{\boldsymbol{\alpha}}^2 \right\rangle}{\sum_{\boldsymbol{\alpha} \in \mathcal{A}, \boldsymbol{\alpha} \neq 0} c_{\boldsymbol{\alpha}}^2 \left\langle \Psi_{\boldsymbol{\alpha}}^2 \right\rangle}, \tag{16}$$

where $\mathcal{A}_i^{\mathrm{total}} = \left\{\boldsymbol{\alpha} \in \mathrm{A} : \alpha_i > 0\right\}$. The benefit of Eqs. (15) and (16) is that, once the PCE surrogate $\mathcal{M}^{\mathrm{PC}}$ is constructed, global sensitivity analysis via Sobol' indices can be conveniently gained by performing simple arithmetic on the coefficients of the PCE surrogate.

For both the main and joint sensitivities, the posterior distribution of the PC coefficients $\mathbf{c}$ are available. It is possible to calculate uncertainty in the sensitivity indices by sampling from the posterior distribution of $\mathbf{c}$ to calculate Eqs. (13)–(16), but this study will use only the mean estimates of the coefficients for sensitivity calculations.

2.4. Parameter inference

Given a suite of results from a mechanistic model $\mathcal{M}$ and its constructed polynomial surrogate $\mathcal{M}^{\mathrm{PC}}$, one can infer which values of uncertain input parameters $\boldsymbol{X}$ are *most likely* to provide results that match an observed quantity. An advantage of the approach outlined here is that $\mathcal{M}^{\mathrm{PC}}$ enables very efficient inverse analysis (Marzouk and Xiu, 2009). More generally, inverse problems occur when there are related observations but they are not necessarily the ultimate quantity of interest. Within hydrology, and particularly in sparsely monitored basins, there is a long history of parameter identification through some form of inversion (e.g., Kirchner, 2009; McLaughlin and Townley, 1996; Neuman et al., 1980; Yeh, 1986). The use of surrogate models with dimension reduction as outlined in the previous sections provides a novel approach, enabling faster computation, inversion, and the ability to solve the inverse problem on a larger set of uncertain model parameters.

As an example, take $\mathbf{u}$ to be a vector of observed data (such as streamflow), and $\boldsymbol{X} = \{X_1, X_2, \cdots, X_M\}$ be the vector of uncertain model input parameters (such as soil hydraulic properties). We further assume that the model gives an adequate approximation of the observed streamflow, $\mathbf{u} \approx \mathcal{M}(\boldsymbol{X})$. The use of Bayes' rule allows for the computation of the posterior parameter values conditioned on the observed data:

$$\Pi(\boldsymbol{X} \mid \mathbf{u}) \propto L(\mathbf{u} \mid \boldsymbol{X}) p(\boldsymbol{X}), \tag{17}$$

where $p(\boldsymbol{X})$ is the prior distribution, $L(\mathbf{u}|\boldsymbol{X})$ is the likelihood function which represents the probability of obtaining the data given the set of parameters, and $\Pi(\boldsymbol{X}|\mathbf{u})$ is the posterior distribution for $\boldsymbol{X}$, which represents the probability of having the parameter values given the observed data.

To formulate a likelihood function, one must represent the discrepancy between the model and observations: $\eta = \mathbf{u} - \mathcal{M}$. Assuming that the components of η are independent and identically distributed random variables with some marginal density p_η, the likelihood function can be written as

$$L(\mathbf{u} \mid \boldsymbol{X}) = \prod_{d=1}^{D} p_\eta(u_d - \mathcal{M}_d(\boldsymbol{X})), \tag{18}$$

where there are D conditions (e.g., time snapshots of measured streamflow, monthly evapotranspiration, etc.) that are being used for inference.

If one assumes, as in this study, that the errors η_d are independent and normally distributed $\eta_d \sim N(0, \sigma^2)$, Eq. (18) can be written as:

$$L(\mathbf{u} \mid \boldsymbol{X}) = \frac{1}{\left(\sqrt{2\pi\sigma^2}\right)^D} \prod_{d=1}^{D} \exp\left[-\frac{(u_d - \mathcal{M}_d(\boldsymbol{X}))^2}{2\sigma^2}\right], \tag{19}$$

where the logarithm of this likelihood function corresponds to the least-squares form of the objective function often used for deterministic parameter estimation (Sargsyan et al., 2015).

If measurements are taken at different times for the observed data series (e.g., streamflow), the variance in error may not be the same at each sampling time and almost surely will not be equal due to temporal variations of streamflow due to hydrologic seasonality. Therefore, it can be valuable to introduce σ^2 as a scalar hyper parameter for the likelihood (Sargsyan et al., 2015) and rewrite the joint posterior distribution of Eq. (17) as

$$\Pi\left(\boldsymbol{X}, \sigma^2 \mid \mathbf{u}\right) \propto \frac{1}{\sqrt{2\pi\sigma^2}} \prod_{d} \exp\left[\frac{-(u_d - \mathcal{M}_d(\boldsymbol{X}))^2}{2\sigma^2}\right] p(X_1) \cdots p(X_n) p(\sigma^2). \tag{20}$$

The prior distribution for the model parameters $p(X_i)$ are based on their *a priori* knowledge, e.g., that the parameters are uniform within a range or normally distributed with some mean and variance. As the variance of the error noise, σ^2 must be positive, we therefore use a Jeffreys prior (Jaynes and Bretthorst, 2003):

$$p(\sigma^2) = \begin{cases} \frac{1}{\sigma^2} & \text{for } \sigma^2 > 0 \\ 0 & \text{otherwise.} \end{cases} \tag{21}$$

To infer values for uncertain model parameters, the posterior distribution from Eq. (20) needs to be sampled using methods such as the Metropolis-Hastings MCMC (MacKay, 1998). Note that sampling from posterior distribution requires repeated evaluation of the likelihood, implying multiple evaluations of the model $\mathcal{M}$. This tends to be computationally expensive, and it is therefore expeditious to replace the model $\mathcal{M}$ with its PCE surrogate $\mathcal{M}^{\mathrm{PC}}$. In this way, the methodology outlined previously in this section can be combined with those in Sections 2.3.1 and 2.3.2 to create a computationally efficient, flexible framework to infer uncertain parameter values for a complex, process-based hydrologic model with multiple inputs applied to sparsely monitored watershed. As in this study, the methodology is able to answer the question of inverse inference: *what is the likely distribution of the model's uncertain parameters given observed data*? Importantly, it is also able to address the question of: *what are the possible outcomes for specific quantities of interest given the uncertainty in the model's inputs*?

2.5. Summary of UQ framework

Sections 2.3–2.4 presents a general framework of high flexibility to infer model parameters for a hydrologic model in a computationally efficient manner by using polynomial surrogates. Fig. 3 provides a diagram outlining this framework. Generally, one uses a hydrologic model to construct a polynomial surrogate model (Box A) that allows for fast computation of output quantities of interest from the hydrologic model. In the case of many uncertain input parameters, dimensionality reduction tools such as BCS are used to alleviate the burden of multi-dimensionality of uncertain inputs for constructing the surrogate models. After a surrogate has been constructed, one can then use it for accelerated, computationally inexpensive inference of the uncertain parameters for the hydrologic model, provided that there are available data matching a quantity of interest (Box B). Once the posterior distributions of the uncertain parameters have been calculated, they can then be used within a model $g(\boldsymbol{X})$. In theory, $g(\boldsymbol{X})$ can be any model that uses the parameters $\boldsymbol{X}$, but it is prudent to use the posterior values in the same model used for inference. Within this study, $g(\boldsymbol{X})$ is going to be tRIBS-VEGGIE ($\mathcal{M}$) in order to estimate other quantities of interest (Section 2.1.5).

A methodological step that accounts for model error is not shown in Fig. 3 and therefore is not accounted for in this study. More specifically, the likelihood function in Box B accounts for *data error*, but does not consider the structural error of tRIBS-VEGGIE. Accounting for model error is an active, ongoing area of research within UQ (e.g., Sargsyan et al., 2018), but is beyond the scope of this study.

The strength of this approach in the context of uncertainty quantification is the relationship between QoIs—as discussed in Section 2.3.1 and observational data. Any QoI can be used for inference, as long as one has a preconstructed PCE surrogate for it. If one can relate observational data to the QoI being addressed through $\mathcal{M}^{\mathrm{PC}}$, then accelerated inference for diverse outputs (e.g., hydrologic, hydraulic, ecologic, biogeochemical, etc.) is possible within complex hydrologic models.

3. Results

This section provides an overview of the results of the construction of the surrogate model from Section 2.3, uses the performance of the surrogate model against observations (Table 1, "Inference" column) to infer parameter values, and relies on the latter to investigate the response of hydrologic variables of interest within the catchment.

The data used to construct the surrogate and perform inference are summarized in Fig. 4. The figure for discharge shows that the model training simulations underestimate the aggregated observed discharge with a small amount of uncertainty associated with the tRIBS-VEGGIE simulations. Water table data are aggregated into groups based on observed well locations (Section 2.1.5), although the simulations generally underestimate water table depth, the uncertainty from the training simulations overlap with the observed data. Simulated evapotranspiration falls within the uncertainty bounds of the observed data, with a slight overestimation of ET during the wet season. Lastly, soil water content is generally overestimated but the uncertainty in the training simulation overlaps the observed data. Ideally, one would like the training simulations to overlap the observed values used for inference, but this is not the case for all QoIs, especially those in the discharge and water table groups. However, Section 3.2 shows how this can be overcome using the inference techniques to better confirm tRIBS-VEGGIE with the observed data.

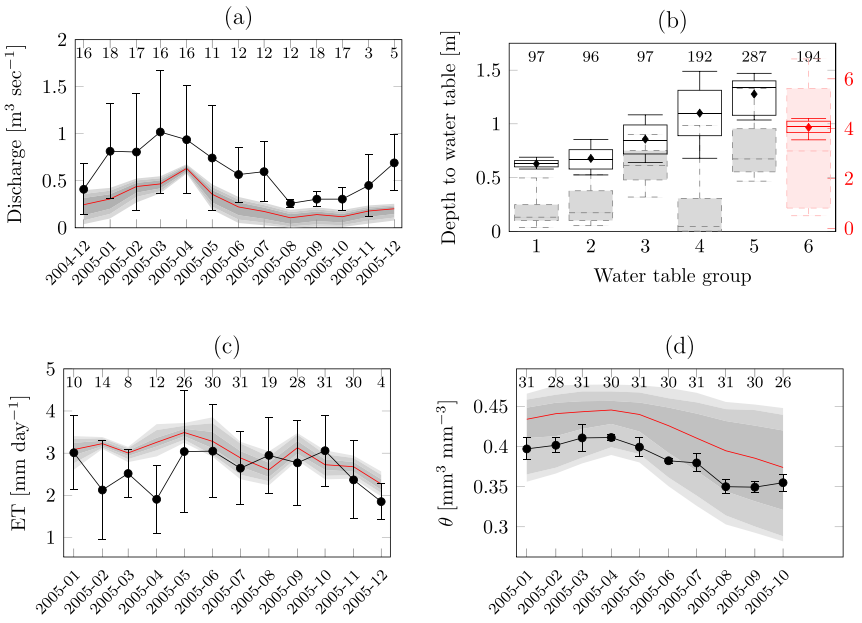

Fig. 4. Plots for observed and training simulations of discharge, depth to water table, evapotranspiration (ET), and soil moisture content (θ). The discharge, ET, and θ figures plot the mean of the time series of available data with the error bars being the standard deviation of the recorded data. The discharge plot also shows the number of records aggregated into each month. Water table depth is displayed in box and whisker plots. The whiskers represent the 10- and 90-percent quantiles, and the box limits represent the 25- and 75-percent quantiles, with the median lying within the box. The diamond within each box is the mean water table value that is used for inference. The shaded regions in the plot represent the training simulations from tRIBS-VEGGIE used to construct the surrogate models. The different shading levels represent the 25/75, 10/90, and 5/95 percentiles of the 100 training simulations. Additionally, the red line used in the time series plots represents the median of the training simulations. The colors within the water table plot are divided into two y-axes to provide better readability and clarity values in groups (1–5) and 6.

3.1. Surrogate construction

The polynomial chaos surrogates $\mathcal{M}^{\text{PC}}$ were constructed as in Eq. (9) for the QoIs in Table 1. To have a well-performing surrogate, $\mathcal{M}^{\text{PC}}$ should match the simulations of the mechanistic model tRIBS-VEGGIE $\mathcal{M}$. In Fig. 5, the absolute errors between the constructed surrogate ($\mathcal{M}^{\text{PC}}$) and training simulations of tRIBS-VEGGIE ($\mathcal{M}$) are shown as illustration. Simulation results used for training purposes of constructing the surrogate are shown. Also shown are the results corresponding to validation of the surrogate, i.e., a comparison of the forward tRIBS-VEGGIE model simulations and outputs of the trained surrogate for the same QoIs.

A quantitative error measure of the surrogate accuracy is the relative L_2-norm as a representation of error, defined as:

$$L_{2,\text{rel}} = \left[\frac{\sum_{i=1}^{N_s} \left(\mathcal{M}_i^{\text{PC}} - \mathcal{M}_i\right)^2}{\sum_{i=1}^{N_s} \mathcal{M}_i^2} \right]^{1/2}, \tag{22}$$

where N_s is the number of training (or validation) simulations performed. The value used for N_s depends on the computational expense of the model, and one would like to have at least 3–4 samples in each uncertain parameter dimension, which in this study would result in at least $3^7 = 2,187$ runs of tRIBS-VEGGIE. To summarize surrogate performance, the QoIs are aggregated into streamflow, water table depth, evapotranspiration, and soil moisture groups. These groups are used to illustrate the relative surrogate error as a function of PC order in Fig. 6, which shows that for training simulations, the decrease in $L_{2,\text{rel}}$ is muted after a PC order of 5 or 6.

We selected a surrogate order $p = 6$ for $\mathcal{M}^{\text{PC}}$ as the optimal order that leads to a sufficiently accurate surrogate without overfitting. Given the seven uncertain input parameters (Table 2), Eq. (10) gives a required $P + 1 = 1,716$ basis terms in $\mathcal{M}^{\text{PC}}$. Only 100 training tRIBS-VEGGIE simulations were used for BCS to construct the surrogate. An additional 10 simulations were used to validate that the constructed surrogate accurately represented the QoIs from tRIBS-VEGGIE. For both the training and validation cases, simulation points were selected via Latin hypercube sampling (McKay et al., 1979).

Qualitatively, Figs. 5 and 6 a both show that the surrogates performs slightly better (i.e., lower values of $L_{2,\text{rel}}$ in Fig. 6) using training rather than validation results. This is the desired behavior as it means that the stopping criteria ϵ from the BCS method (Section 2.3.2, Appendix A) are chosen correctly. In the case where reducing ϵ improves the performance (reduction in $L_{2,\text{rel}}$) at the training set, but at the expense of performance at the validation set, overfitting has occurred in surrogate training. This means that the surrogate is being trained to only capture the behavior near the parameter samples at the training locations, and will not accurately capture the behavior at a significant distance away from these training samples. Evidence of overfitting would be that $L_{2,\text{rel}}$ decreases with training data but remains the same or increases in the validation data set. This is what occurs if higher-order terms in the expansion are retained for most groups of QoIs.

3.1.1. Sensitivity analysis

Using a constructed PCE model allows for efficient computation of the main and joint effect sensitivity indices from Equations (13) and (14). One can assess the sensitivity contributions for a single QoI, or for uncertain parameters across multiple QoIs.

For the first instance, the main and joint sensitivities of the uncertain parameters for the QoIs of water table group 5 and evapotranspiration in April 2004 are shown in Fig. 6c and d, respectively. The main effect sensitivities — the fraction of variance described by changing each uncertain parameter in isolation, averaged over the input distribution of the other parameters — are given on the diagonal of these figures. For the water table and evapotranspiration groups, one sees that k_{sat} is the dominant contributor in the variation of the QoIs shown. This displays that the model is qualitatively consistent, as a higher value of saturated conductivity allows faster drainage from the soil and impacts water available for vegetation transpiration in the case of Fig. 6d. The lower diagonal on Fig. 6c and d represents the joint effect sensitivities, e.g., in Fig. 6c, terms in the expansion containing both k_s and a_r account for approximately 9.5% of the variability seen in the fifth water table group, while the equivalent contribution from terms containing both a_r and F_C is approximately 0.45%. Recalling from Eqs. (15) and (16), these sensitivities are computed directly from the PCE coefficients, so sparsity or very low values in the lower diagonal (e.g., Fig. 6c) represents zero or near-zero values of the coefficients multiplying terms containing the uncertain parameters. The implication of this sparsity is that interaction between those parameters in the model have an insignificant impact on the resultant value of the QoI.

These indices are computed for each QoI, and summarized sensitivities across all QoIs are given in Fig. 6b. Based on the contributions to the variances of the QoIs, it is clear that k_{sat} is the uncertain parameter with

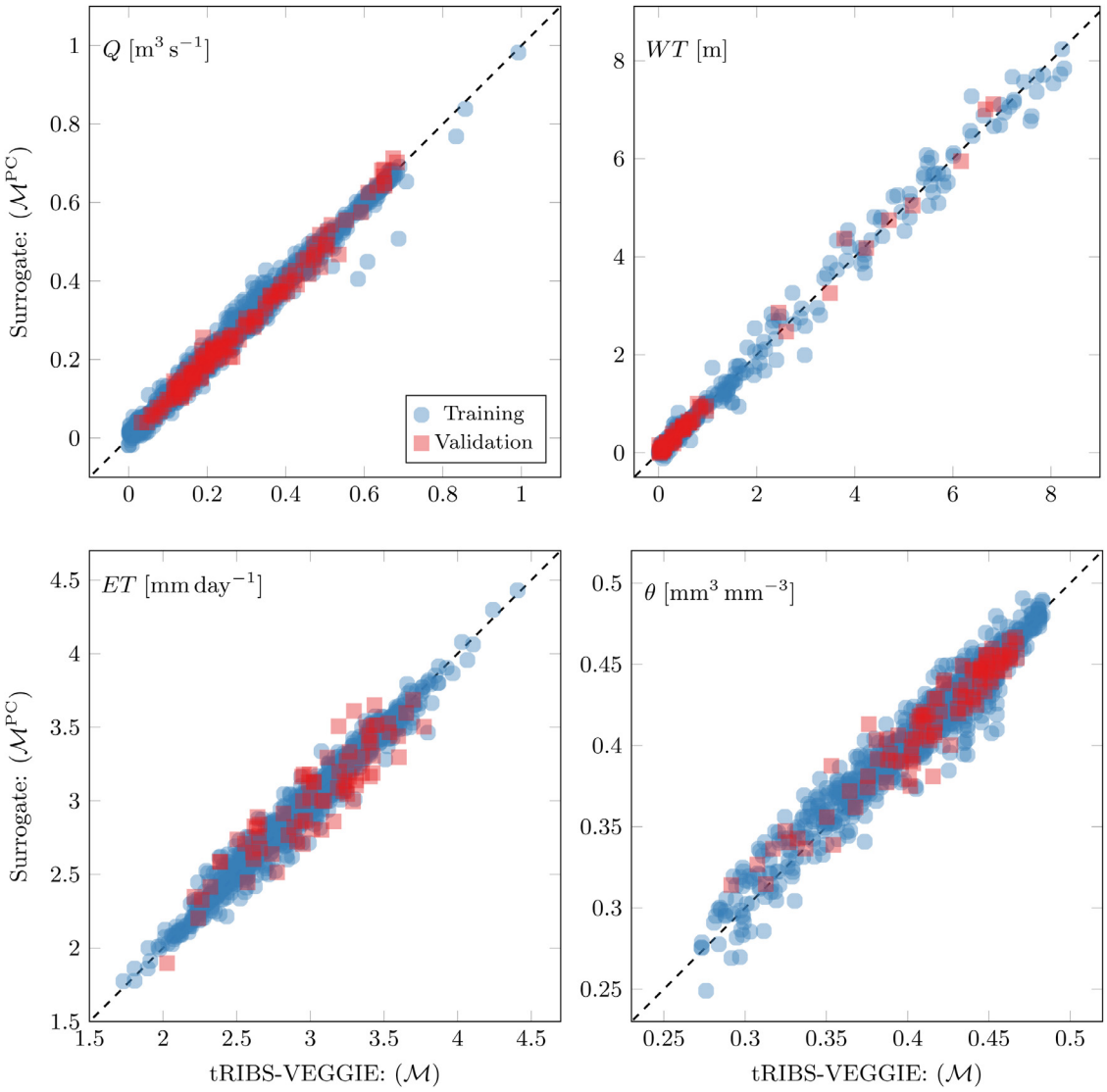

Fig. 5. Comparison of tRIBS-VEGGIE and constructed surrogate for PC order $p = 6$. The surrogates are separated into four groups depending on the QoI. Blue circular and red square marks represent the 100 training and 10 validation simulations, respectively. A $y = x$ line is added to each plot, such that points on the black line represent agreement between tRIBS-VEGGIE and the constructed surrogate. The relative errors of the surrogates for each group are: $L_{2,\text{rel}}(Q) = 0.081$, $L_{2,\text{rel}}(WT) = 0.10$, $L_{2,\text{rel}}(ET) = 0.025$, and $L_{2,\text{rel}}(\theta) = 0.029$.

the largest impact on model sensitivity for the identified QoIs. This confirms intuition since values of k_{sat} control both infiltration excess runoff as well as impact of lateral flows in the hydrologic system, which is not included in the pedotransfer function of Tomasella et al. (2000). Those parameters which are included in the pedotransfer function change the shape of soil water retention curve. Therefore, sensitivity to these parameters (F_C, F_S, α_{CS}, M_e, ρ_b) indicates sensitivity of QoIs to the water retention characteristics of the soil.

3.2. Inference of soil properties

After the surrogate model is obtained, it is possible to calculate the posterior distribution of model parameters through MCMC sampling, as described in Section 2.4, by replacing $\mathcal{M}$ with $\mathcal{M}^{PC}$. This enables faster computation and benefits hydrologic models that take more than a few minutes to perform a single simulation. The marginal and pairwise marginal posterior distributions of the hydrologic parameters in Table 2 are shown in Fig. 7. These marginal posterior distributions are summarized in Table 3 by their moments, *maximum a posteriori* (MAP) estimate, i.e., the mode of the posterior distribution, and the coefficient of variation (ratio of standard deviation to the mean value).

These posterior distributions provide information about the bulk soil properties of the watershed, e.g., that the soil is mostly clay and silt, with a saturated conductivity around 20 [mm/h], and an accompanying anisotropy ratio of approximately 1.25. These values are in agreement with previous studies of the catchment (e.g., Cuartas et al., 2012; Tomasella et al., 2008), which found four different soil types within the watershed. The clay contents for these four soil types (below 1 [m]) ranged between 5 and 90% clay, where the soil type with 80–90% clay accounting for 45% of the catchment, and the soil type with 5% clay accounting for 30% of the catchment. Using a single soil type in the catchment represents an aggregation of the physical properties, whereby the posterior mean for clay content of 56% is reasonable based on the observed properties. The other parameters of the pedotransfer function fall within ranges given in Tomasella et al. (2000), with additional qualitative agreement between the textural classification shown for Manaus, located south of the case study Asu watershed. The hydraulic properties of k_s and a_r in Cuartas et al. (2012) have sixteen classifications based on landscape classes and depth, with the inferred

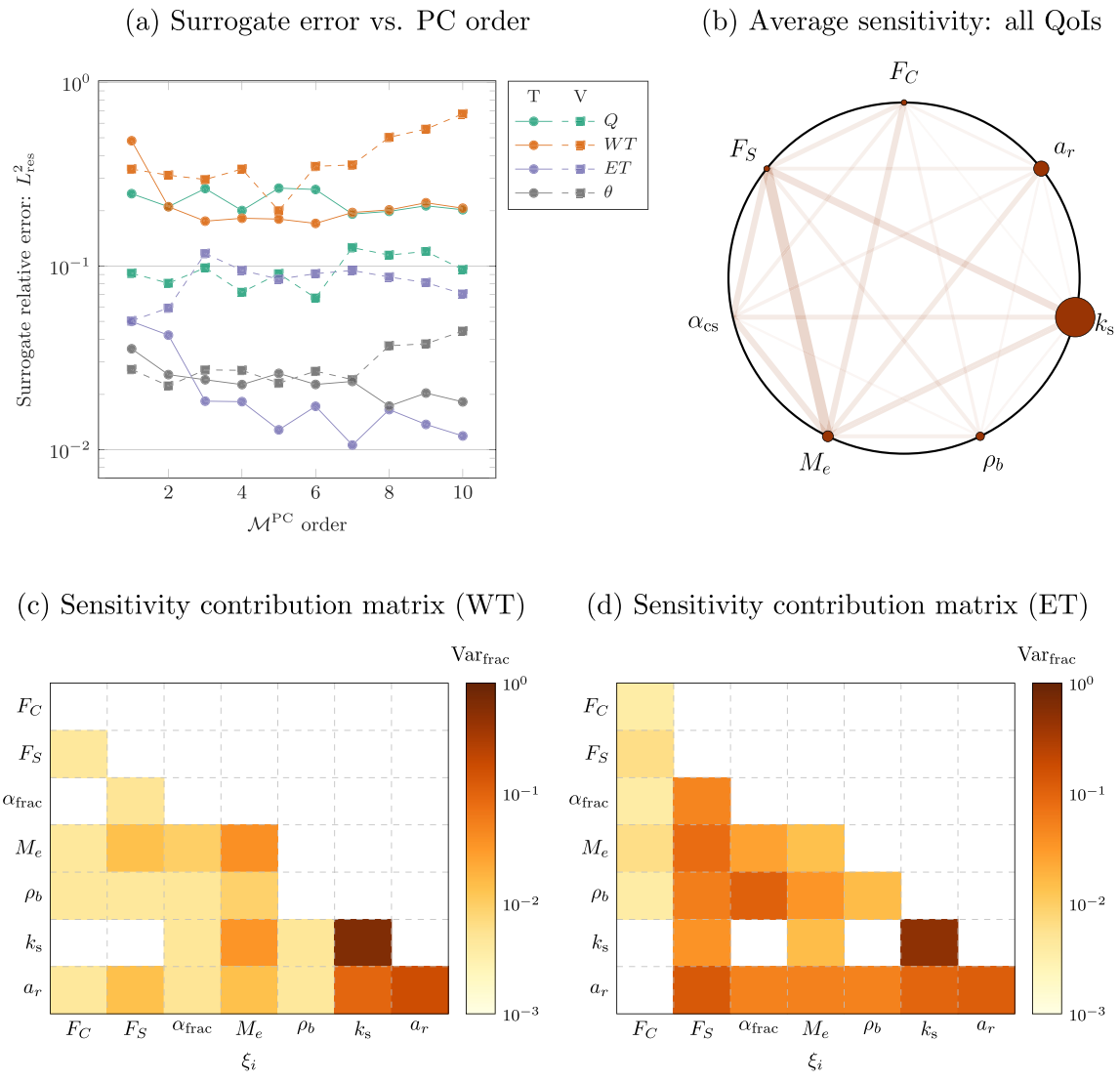

Fig. 6. Plots of surrogate errors and sensitivities. The training and validation surrogate error is given in (a). Each color represents a different group of QoIs, and the marker shape differentiates between training and validation samples. A qualitative representation of sensitivities is given in (b). Here, the diameter of the nodes around the circle are proportional to the main effect sensitivities, and the width and opacity of the lines connecting the nodes around the circle are proportional to the joint sensitivities, where the main and joint sensitivities are calculated for each QoI, and the plot shows the average over all QoIs. The lower triangular matrices in (c) and (d) show the main and joint sensitivities for water table group 5 (c) and evapotranspiration in April, 2005 (d). The main effect sensitivities are on the diagonal, and joint sensitivities between parameters are lower triangular, with a minimum sensitivity threshold of 10^{-5}.

values in this study indicating a soil type similar to the "plateau" or "slope" landscape which are at least 15 [m] above the nearest stream node, accounting for approximately 45% of the catchment area. Similarly, Fang et al. (2017) contains hydraulic properties with a single landscape classification at four depths, where k_s is approximately between 9 and 15 [mm/h] with $a_r = 1$, which qualitatively agrees to the inferred value of 15.8 [mm/h]. Additionally, one can assess the pairwise correlations between parameters using Fig. 7, e.g., that the anisotropy ratio (a_r) is negatively correlated with saturated conductivity (k_s).

Posterior predictions of the QoIs are demonstrated in Fig. 8. Here, the joint posterior distribution from Fig. 7 is sampled in order to calculate the QoI values using the surrogates constructed in Section 3.1. A comparison can then be made between the posterior QoI values and the observed data values. One sees that the posterior QoIs for ET and soil moisture match the data better than for discharge and depth to water table. There are two main factors contributing to this: (1) the simulated (using $\mathcal{M}$) ET and soil moisture match the corresponding observations better than the simulated discharges and water table depths (see Fig. 4), and (2) data noise for these QoIs are much lower than those for discharge. Nonetheless, one may attempt to improve the skill, if it is deemed unacceptably low. If one were interested in getting a better fit to the data for a set of QoIs, one could: (i) select a larger training set to have more chances for the simulation results of $\mathcal{M}$ to match observations; (ii) perform inference using a subset of the observed data and QoIs, in an attempt to exclusively fit for that subset of data (e.g., see a discussion below in relation to Fig. 9); or (iii) attempt to collect more data to constrain the data noise. In the cases of options (ii) and (iii), the PCE framework provides a benefit of not needing to rerun simulations of the computationally-expensive $\mathcal{M}$, but also allows fine-tuning of model parameters for investigations into specific QoIs.

Modeling factors impacting the difference between, and the uncertainty of, simulated and observed quantities include spatial resolution and soil property variability. The watershed used in this study has a steep transition between the plateau and lowland areas (Chauvel et al., 1987; Cuartas et al., 2012). The slopes caused by this transition, in conjunction with the 90 [m] spatial discretization, end up creating a "resolution effect" for quantities such as ground water. The horizontal position of the water table well within the computational cell can impact

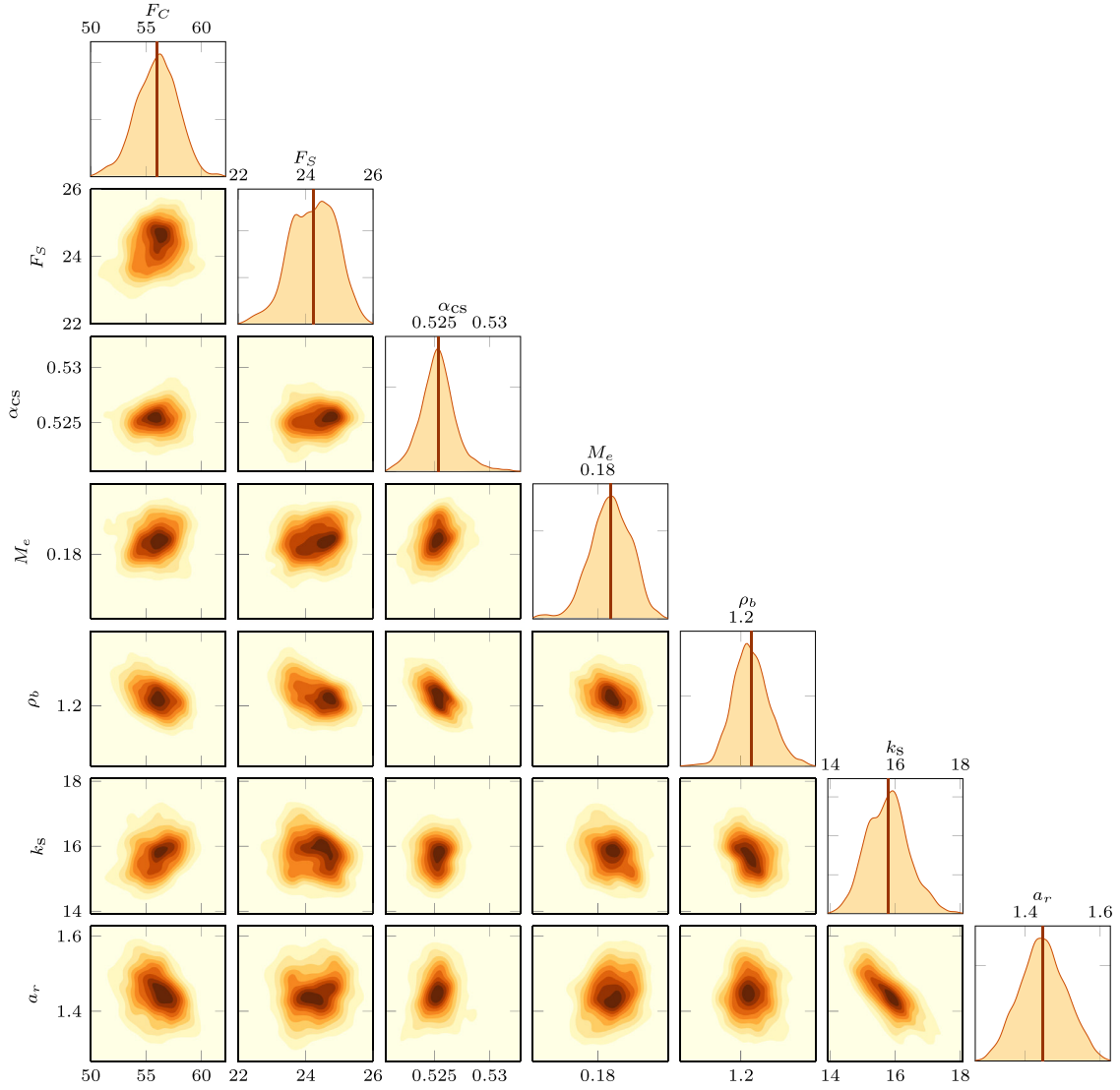

Fig. 7. Posterior distributions of parameters used in inference. The vertical line in each of the diagonal is the estimated mean of the posterior distribution. Summary statistics for the marginal distributions are given in Table 3.

Table 3
First two moments and MAP estimate of parameter posterior distributions.

X_i	$\hat{\mu}$	$\hat{\sigma}$	MÂP	$\hat{\sigma}/\hat{\mu}$ [%]
F_c	56.0	1.871	56.3	3.34
F_S	24.2	0.677	24.5	2.79
α_{CS}	0.525	1.64E-3	0.525	0.31
M_e	0.184	5.75E-3	0.184	3.13
ρ_b	1.2	1.19E-3	1.2	9.9E-2
k_s	15.8	0.645	15.9	4.09
a_r	1.45	6.11E-2	1.44	4.22

its agreement to observed water table depths. Additionally, the channel is represented within the model using the 90 [m] cells, and the lack of an incised channel means that drainage from the saturated zone to the channel is less efficient. All quantities also could have been affected by the lack of spatial variability in soil properties. Four soil types are reported for this watershed in Cuartas et al. (2012), with one representative soil type being used in this study. As a result, quantities that are measured at specific locations (water table depth, evapotranspiration, and soil moisture content) are likely affected by this modeling choice.

The posterior QoIs as a result of performing inference separately on each group of QoIs (i.e., only data of a given group are used to infer the entire set of parameters in Table 2) are shown in Fig. 9. In this figure, the data noise—σ^2 in Eq. (20) was set as a hyper-parameter and was also inferred because it provides a better fit of the mean prediction of $\mathcal{M}^{PC}$ to the data. This was done to illustrate an approach that can be undertaken when data noise is large to the point of observations becoming uninformative, e.g., in the case of discharge and ET data. In this case a Jefferys prior (Eq. (21)) is used for σ^2. Performing inference on each group of QoIs is done at the expense that the parameter posterior distributions become specific for each separate group of QoIs. The posterior distribution in Fig. 9 for the variables X_i contain other important details about the information that can be gained with inference. For example, the marginal posterior distribution for the bulk density (ρ_b) is very close to the uniform prior distribution for most groups of QoIs, since this parameter is not informed by the available data (except for soil moisture).

Whether one takes the approach shown in Fig. 8 or 9 will depend on the questions being investigated. Generally, the Bayesian framework prefers including all data to perform inference, as long as the data are informative. In the case where data come from disparate sources, e.g., sporadic sampling of discharge vs. hourly evapotranspiration measurements, one may want to separate the inference using these data, or incor-

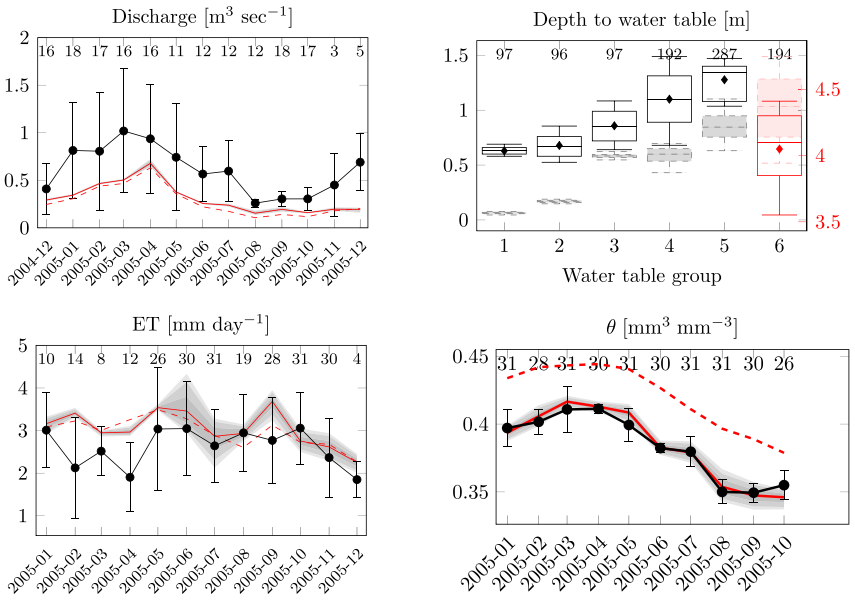

Fig. 8. Plots for observed discharge, depth to water table, evapotranspiration (ET), and soil moisture content (θ) compared to surrogate calculations using the samples of posterior distribution from Fig. 7, which are summarized in Table 3. The dashed red line corresponds to the median training simulation values as in Fig. 4, while the solid red line represents the median values of the surrogate simulations with the posterior parameter samples. Please refer to Fig. 4 for a description of other presentation details.

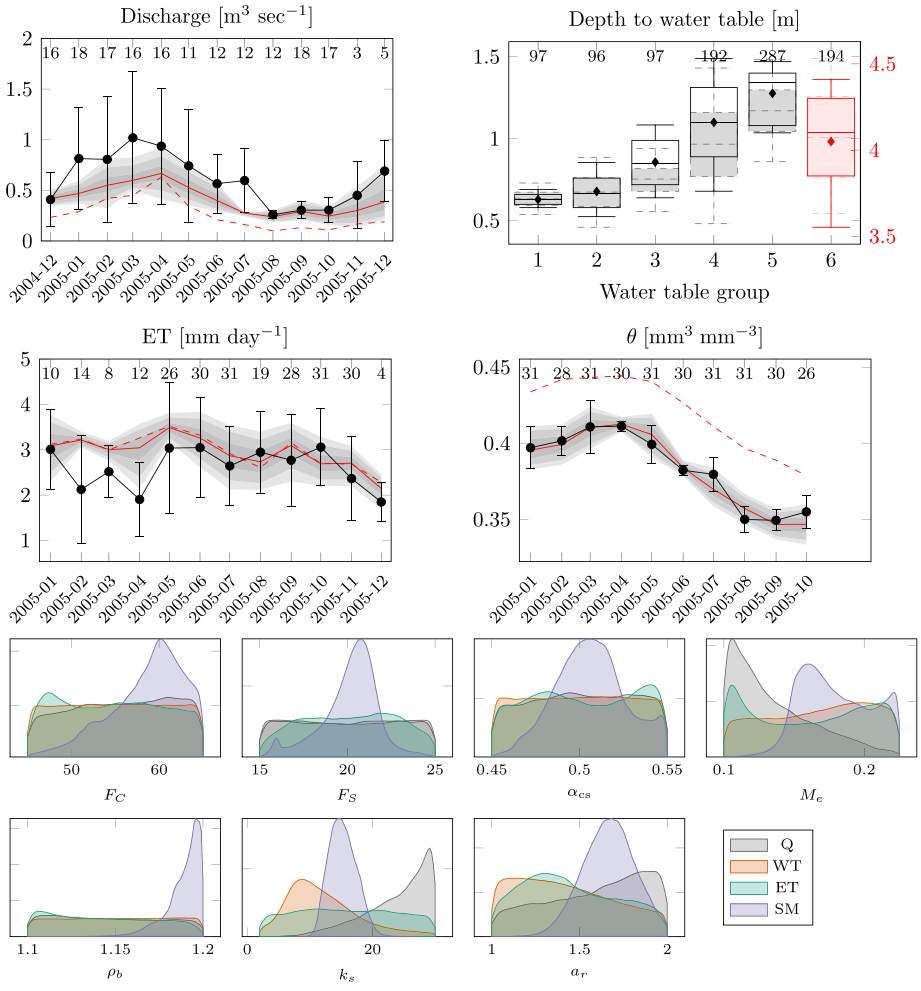

Fig. 9. Plots for the four output groups of observed discharge, depth to water table, evapotranspiration (ET), and soil moisture content (θ) compared to surrogate calculations using posterior parameter values that were inferred for each individual output group. This path of inference generates four separate posterior PDFs for $\boldsymbol{X}$, which are shown at the bottom of the figure. The dashed red line corresponds to the median training simulation values as in Fig. 4, while the solid red line is the median value of the surrogate simulations with the posterior parameter samples. For each output group, the grey regions represent the 95% uncertainty bound from propagating the parameter posteriors for that output group (Q, WT, ET, SM) through the respective surrogates.

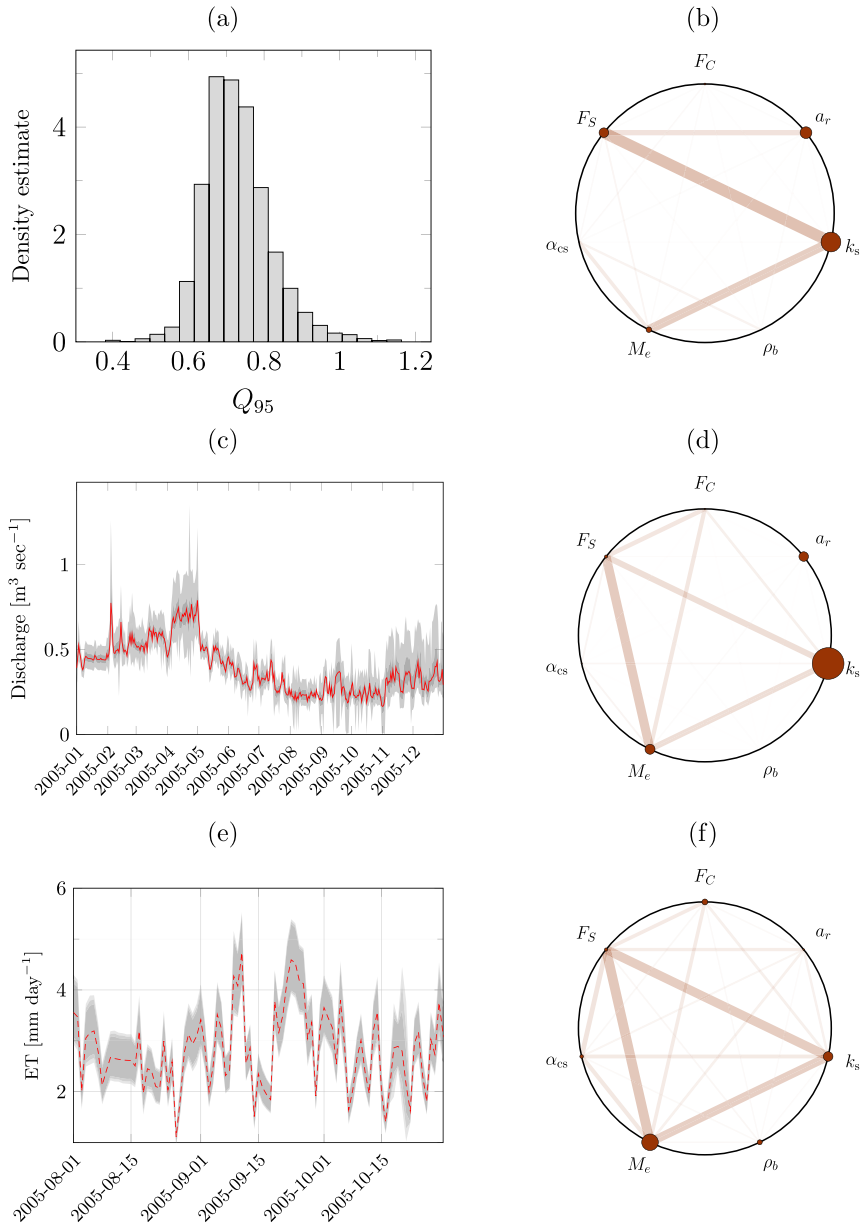

Fig. 10. Posterior QoIs (left) and their sensitivities (right) corresponding to the QoIs not included in inference in Table 1, due to insufficiency/lack of observational data. The surrogates for these QoIs were constructed using the same 100 training and 10 validation simulations as in Fig. 4. In plots (c) and (e), the grayed region represents the 5% and 95% quantiles of surrogate simulations evaluated using the posterior parameter distributions in Fig. 9. See Fig. 6b for details on the representation of sensitivities in (b), (d), and (f).

porate more detailed structure in the data noise representation among groups of QoIs to better inform their impact on inference.

3.3. Computing QoIs from posteriors

With the framework presented in this study, one can construct a surrogate model for quantities that have been observed (Section 3.1) and use this surrogate to confirm the model's behavior (Section 3.2). This allows one to investigate a wide variety of model behaviors, such as higher-frequency or aggregated quantities at coarser or finer temporal/spatial intervals. In this work, the parameter posterior distribution from Fig. 9 resulted in a chain of 19,000 posterior values for each parameter in Table 2, which can be directly sampled and used as input to a constructed surrogate (box (C) in Fig. 3).

From Table 1, the QoIs held out from inference were: Q_{95} — the 95th percentile of *daily-averaged* discharge during 2005 (representing the probability that 18 days during the year have a mean daily discharge larger than Q_{95}), $\mathcal{T}S(Q)$ — the daily time series of streamflow in 2005, and $\mathcal{T}S(ET_{\text{dry}})$ — daily evapotranspiration in months with cumulative water deficit as defined in Eq. (1). Illustration plots and sensitivity information for these QoIs are given in Fig. 10. Note that the surrogates for these higher-frequency and aggregated QoIs were not constructed in Section 3.1, but doing so is straightforward and follows the methodology of Section 2.3.1.

These results are provided to illustrate the flexibility of the UQ framework. The benefits of the approach include that one can investigate hydrologic response at higher temporal and spatial resolutions. For example, one can see the pattern of discharge in Fig. 10 follows that of Fig. 9, but unlike the original data sourced in Fig. 4, the illustration provides daily estimates of discharge.

4. Discussion

Despite recent advances in computational power, simulation times for complex, process-rich hydrologic models, even for low-order catchments can be significant. When a large number of uncertain parameters or, generally, uncertain model inputs are used, thousands of model simulations may be required to perform robust, comprehensive un-

certainty quantification, parameter inference, and sensitivity assessment. Even reduced-order simulation approaches recently introduced to earth-system and environmental modeling would be prone to computational issues. This study addresses this challenge and adopts an efficient methodology to enable uncertainty quantification and stochastic simulation with deterministic, process-based hydrologic models of higher complexity. This work applies recent developments that combine reduced-order modeling based on polynomial chaos expansions with Bayesian compressive sensing to construct computationally cheap surrogate formulations of the complex hydrologic model, while significantly reducing the number of required simulations. The surrogate representation enables Bayesian inversion and calibration of uncertain model variables for any model output that can be compared to observable data, even when these are sporadic and have time-varying accuracy. Furthermore, surrogate formulation can be used to propagate uncertainty through a hydrologic model for any of the model's outputs, enabling one to estimate uncertainties of QoIs that are difficult or too costly to measure.

A limitation of this study is the intentionally constrained nature of possible sources of input uncertainty included in the analysis. As mentioned in Section 2.3, one can use both parametric and input spatial field uncertainty within the UQ framework. The parametric type was chosen to display a clear presentation of how uncertainty can be addressed using a complex model. This approach however does not limit an extension of the analysis to other uncertain variables or spatial fields. For instance, the incorporation of the uncertainty in spatial or temporal fields is important to determine hydrologic response (Kim et al., 2019). An approach to address this uncertainty within the framework includes creating a stochastic model of the uncertain field using a Karhunen–Loéve expansion (Karhunen, 1946; Zheng and Dai, 2017). This decomposes the uncertainty in the spatial field into a parametric stochastic model, where the uncertain parameters can be included into $\boldsymbol{X}$. Following this philosophy, uncertain soil moisture, precipitation, or water table fields could be propagated through a hydrologic model. This is beyond the scope of the current study and will be addressed in future research. Furthermore, there is evidence suggesting that multiple soil types are present in the study domain (e.g., Cuartas et al., 2012; Tomasella et al., 2008), while a single soil type was used in this work. This design choice was undertaken for two reasons: i) to represent the more typical case in hydrology of not having detailed soil data available, and ii) for an unobscured, clean presentation of the methodology without extraneous details that would arise from using multiple soil parameter sets. If finer detail of soil representation were included, one would expect inference and sensitivity to be weighted to the spatial coverage of soil types. For example, the hydraulic conductivity of a soil type controlling infiltration of precipitation into the subsurface would have a greater contribution to the variation of streamflow if the soil type covered 50% rather than 10% of the watershed. Another limitation is the current version of the model used in this study, tRIBS-VEGGIE, has a limited capability to incorporate vertical heterogeneity to the soil column.

The approach is flexible, and relies on *a priori* identification of input variables of high impact before modeling. This means that although one can change the QoIs being investigated by working with the model's output, one cannot change the parameters that are treated as uncertain without having to rerun training and validation simulations. Given the reduction in computational expense due to the use of the Bayesian compressive sensing methodology, it is possible to treat dozens of model parameters as uncertain (Ricciuto et al., 2018; Sargsyan et al., 2014), essentially assuming no *a priori* knowledge of impactful variables. However, in most cases in hydrology, it is beneficial to constrain the number of uncertain parameters using expert knowledge about the governing processes controlling QoIs and the respective variables impacting these processes. Alternatively, one can do an initial screening of model parameters with Bayesian compressive sensing. This will not produce an accurate surrogate, but will yield accurate sensitivities, so the parameter space can be reduced and the procedure repeated to gain a more accurate surrogate.

Given the scale and complexity of environmental systems, one must include uncertainty if one hopes to capture or discover complex hydrologic behavior. Uncertainties are ubiquitous within the field of hydrology, e.g., a measurement of a basin-aggregated metric such as streamflow (Fig. 4) is subject to uncertainty within the catchment. Or there may be interactions with model input variables, meaning that to best capture reducible uncertainty about variables, description through probability densities (Fig. 7) is preferred over scalar, deterministic values. In either case, the presented approach offers a novel, sufficiently general way forward to address uncertainties in hydrology, reducing or defining the uncertainties of model inputs.

Generally, the framework outlined in this study provides flexibility to address computationally expensive problems in hydrology (e.g. high-resolution modeling of soil moisture (Ivanov et al., 2010; Krasnosel'skii and Pokrovskii, 1989), representation of macroporosity (e.g., Beven and Germann, 1982), etc.) by enabling high-fidelity simulations under uncertainty. In the cases where these simulations are highly sensitive to input parameters *and* forcings, the presented approach can be applied to high-dimensional parameterized input $\boldsymbol{X}$.

Relevant software tools have been developed in recent years, so that the hydrologist need not also be an expert in uncertainty quantification to apply these methodological approaches. Those that are freely available for research use and actively developed include the Uncertainty Quantification Toolkit (UQTk) (Debusschere et al., 2017, version 3.0.4 used in this study), UQLab (Marelli and Sudret, 2014), and the MIT Uncertainty Quantification Library (Parno et al., 2014).

Acknowledgments

The study was funded by the National Science Foundation grant EAR 1151443 "CAREER: A Multi-Scale Approach to Assessment of Climate Change impacts on Hydrologic and Geomorphic Response of Watershed Systems within an Uncertainty Framework," the DOE Office of Science Graduate Student Research award 33165, DOE Award DE-SC0011078 "Understanding the Response of Photosynthetic Metabolism in Tropical Forests to Seasonal Climate Variation", the "Catalyst Program" of the Michigan Institute for Computational Discovery and Engineering at the University of Michigan, and by the NSF grant 1725654 to V. Ivanov. J. Kim was supported by a grant (19AWMP-B127554-03) from the Water Management Research Program funded by Ministry of Land, Infrastructure and Transport of the Korean government. Special thanks to Sandia National Laboratories and the Uncertainty Quantification group for their help with navigating UQ and UQTk. Sandia National Laboratories is a multimission laboratory managed and operated by National Technology and Engineering Solutions of Sandia, LLC., a wholly owned subsidiary of Honeywell International, Inc., for the U.S. Department of Energy's National Nuclear Security Administration under contract DE-NA-0003525. The U.S. Department of Energy Office of Biological and Environmental Research supported the Next Generation Ecosystem Experiment (NGEE) Tropics project that provided the data used for model simulations (available through the Pacific Northwest National Laboratory). We would like to acknowledge the generous support of the Large Scale Biosphere-Atmosphere (LBA) Program in the Amazon by the National Institute for Amazonian Research (INPA). We also would like to thank Marciel Jose Ferreira and Bruce Nelson at the Department of Forest Sciences, Federal University of Amazonas, Manaus, Amazonas, Brazil. The authors are thankful to two anonymous reviewers for their constructive comments that significantly improved the manuscript.

Appendix A. Bayesian compressive sensing for surrogate construction

The BCS approach provides marginal posterior probability distributions of the vector of coefficients in the PCE model, $\mathbf{c} = \{c_0, c_1, \dots, c_P\}$. Given available data D, Bayes' formula (Jaynes and Bretthorst, 2003)

for this situation can be written as

$$q(\mathbf{c}) \propto L_D(\mathbf{c})p(\mathbf{c}), \tag{A.1}$$

where $q(\mathbf{c})$ is the posterior distribution, $p(\mathbf{c})$ is the distribution representing prior information on the PC coefficient vector $\mathbf{c}$, and $L_D(\mathbf{c})$ is the likelihood function, i.e., a measure of goodness-of-fit for the PCE surrogate model $\mathcal{M}^{\mathrm{PC}}$ from Eq. (9) to the fully deterministic model $\mathcal{M}$. Assuming a Gaussian noise model with a standard deviation σ representing a tolerance of the discrepancy between $\mathcal{M}^{\mathrm{PC}}$ and $\mathcal{M}$ for the likelihood:

$$L_D(\mathbf{c}) = (2\pi\sigma^2)^{(-N/2)} \exp\left[-\sum_{k=1}^{N} \frac{\left(\mathcal{M}_k - \mathcal{M}_{\mathbf{c}}^{\mathrm{PC}}(\boldsymbol{X}_k)\right)^2}{2\sigma^2}\right], \tag{A.2}$$

where $k = 1, \ldots, N$ correspond to realizations of the random input parameters $\boldsymbol{X}$. Note that Eq. (A.2) implies independence of marginal likelihood functions.

The prior distribution $p(\mathbf{c})$ represents prior information on the PC coefficient vector $\mathbf{c}$, the posterior distribution $q(\mathbf{c})$ is the outcome of the inference given the data set D. In the case of PCEs, the prior information of $\mathbf{c}$ should be flat, so no knowledge is assumed in the calculation of the posterior distribution for $\mathbf{c}$. A flat prior distribution is preferred because the use of BCS motivates that many of the terms in $\mathbf{c}$ will be very close to zero, leading to a lower number of polynomial basis terms that give valuable information for the expansion in Eq. (9).

Achieving a sparse posterior distribution is strongly supported by sparse priors that give vanishing values for the coefficients unless there is strong evidence to the contrary. As such, this study uses the sparse Laplace prior Babacan et al. (2010), that assumes coefficient independence:

$$p(\mathbf{c}) = \left(\frac{\beta}{2}\right)^{P+1} \exp\left(-\beta \sum_{j=0}^{P} |c_j|\right), \tag{A.3}$$

where β is a positive shape parameter that also controls the optimization problem in Eq. (A.4). The vector $\mathbf{c}$ that maximizes the posterior distribution $q(\mathbf{c})$ is given by the solution to

$$\underset{\mathbf{c}}{arg\,max}\left(\log L_D(\mathbf{c}) - \beta||\mathbf{c}||_1\right), \tag{A.4}$$

which is the compressive sensing algorithm used in signal processing (Candès et al., 2006), where the $-\beta\|\mathbf{c}\|_1$ term is due to the l_1 norm-based regularization approach in BCS. The regularization approach is used to reduce overfitting while learning the coefficients $\mathbf{c}$. Different approaches would lead to different regularization terms in Eq. (A.4). Details of the implementation of this approach are left to Sargsyan et al. (2014), but one of the key points is the selection of stopping criterion. Specifically, the algorithm iterates finding the basis terms $\mathbf{c}$ until it reaches a stopping criterion ϵ comparing the relative change in the maximal value of the evidence E — the integrated likelihood. The stopping criterion is defined as $(E^n - E^{n-1})/(E^n - E^1) < \epsilon$, where n is the iteration number. As ϵ decreases, more iterations are required, meaning that fewer basis terms are retained in the final polynomial surrogate. A discussion on the selection of ϵ is included in Section 3.1.

For example, in Sargsyan et al. (2014), the Community Land Model with carbon-nitrogen cycling (Thornton et al., 2007) was modeled with 79 uncertain input parameters, where second, third, and fourth-order polynomials lead to order 10^3, 10^5, and 10^6 basis terms, respectively. Using 10,000 model simulations, the BCS methodology demonstrated an excellent performance skill for a very large uncertain parameter set by avoiding the calculation of all these basis terms and selecting only those relevant to the QoIs. During testing, 17 model simulations failed resulting in 9983 simulations used for training the surrogate model. This displays another advantage of the BCS method, as failed simulations do not limit the solution of the coefficients as it would in quadrature methods. The methodology also allows additional simulations to be added if an initial simulation set is determined to be insufficient to train the surrogate model.

Supplementary material

Supplementary material associated with this article can be found, in the online version, at doi:10.1016/j.advwatres.2019.01.002.

References

Abbaspour, K.C., Johnson, C.A., Van Genuchten, M.T., 2004. Estimating uncertain flow and transport parameters using a sequential uncertainty fitting procedure. Vadose Zone J. 3 (4), 1340–1352.

Abril, G., Martinez, J.-M., Artigas, L.F., Moreira-Turcq, P., Benedetti, M.F., Vidal, L., Meziane, T., Kim, J.-H., Bernardes, M.C., Savoye, N., Deborde, J., Souza, E.L., Albéric, P., Landim de Souza, M.F., Roland, F., 2014. Amazon River carbon dioxide outgassing fuelled by wetlands. Nature 505 (7483), 395–398. https://doi.org/10.1038/nature12797.

Ajami, H., McCabe, M.F., Evans, J.P., Stisen, S., 2014. Assessing the impact of model spin-up on surface water-groundwater interactions using an integrated hydrologic model. Water Resour. Res. 50 (3), 2636–2656. https://doi.org/10.1002/2013WR014258.

Ascough Ii, J.C., Maier, H.R., Ravalico, J.K., Strudley, M.W., 2008. Future research challenges for incorporation of uncertainty in environmental and ecological decision-making. Ecol. Modell. 219 (3–4), 383–399.

Babacan, S., Molina, R., Katsaggelos, A., 2010. Bayesian compressive sensing using laplace priors. IEEE Trans. Image Process. 19 (1), 53–63. https://doi.org/10.1109/TIP.2009.2032894.

Bear, J., 1979. Hydraulics of Groundwater. McGraw-Hill International Book Co.

Beighley, R.E., Eggert, K.G., Dunne, T., He, Y., Gummadi, V., Verdin, K.L., 2009. Simulating hydrologic and hydraulic processes throughout the Amazon River Basin. Hydrol. Processes 23 (8), 1221–1235.

Berveiller, M., Sudret, B., Lemaire, M., 2006. Stochastic finite element: a non intrusive approach by regression. Eur. J. Comput. Mech. 15 (1–3), 81–92. https://doi.org/10.3166/remn.15.81-92.

Beven, K., 1982. On subsurface stormflow: an analysis of response times. Hydrol. Sci. J. 27 (4), 505–521.

Beven, K., 1993. Prophecy, reality and uncertainty in distributed hydrological modelling. Adv. Water Resour. 16 (1), 41–51. https://doi.org/10.1016/0309-1708(93)90028-E.

Beven, K., 2013. So how much of your error is epistemic? Lessons from Japan and Italy. Hydrol. Processes 27 (11), 1677–1680. https://doi.org/10.1002/hyp.9648.

Beven, K., Germann, P., 1982. Macropores and water flow in soils. Water Resour. Res. 18 (5), 1311–1325.

Beven, K., Westerberg, I., 2011. On red herrings and real herrings: disinformation and information in hydrological inference. Hydrol. Processes 25 (10), 1676–1680. https://doi.org/10.1002/hyp.7963.

Beven, K.J., Almeida, S., Aspinall, W.P., Bates, P.D., Blazkova, S., Borgomeo, E., Goda, K., Phillips, J.C., Simpson, M., Smith, P.J., 2016. Epistemic uncertainties and natural hazard risk assessment–part 2: different natural hazard areas. Nat. Hazards Earth Syst. Sci. 2016 (1). 1–1.

Beven, K.J., Aspinall, W.P., Bates, P.D., Borgomeo, E., Goda, K., Hall, J.W., Page, T., Phillips, J.C., Rougier, J.T., Simpson, M., 2015. Epistemic uncertainties and natural hazard risk assessment–part 1: a review of the issues. Nat. Hazards Earth Syst. Sci. Discuss 3 (12), 7333–7377.

Bisht, G., Huang, M., Zhou, T., Chen, X., Dai, H., Hammond, G.E., Riley, W.J., Downs, J.L., Liu, Y., Zachara, J.M., 2017. Coupling a three-dimensional subsurface flow and transport model with a land surface model to simulate stream – aquifer – land interactions (CP v1.0). Geosci. Model Dev. 10 (12), 4539–4562. https://doi.org/10.5194/gmd-10-4539-2017.

Blatman, G., Sudret, B., 2008. Sparse polynomial chaos expansions and adaptive stochastic finite elements using a regression approach. Comptes Rendus Mécanique 336 (6), 518–523.

Blatman, G., Sudret, B., 2011. Adaptive sparse polynomial chaos expansion based on least angle regression. J. Comput. Phys. 230 (6), 2345–2367.

Broedel, E., Tomasella, J., Cândido, L.A., von Randow, C., 2017. Deep soil water dynamics in an undisturbed primary forest in central Amazonia: differences between normal years and the 2005 drought. Hydrol. Processes 31 (9), 1749–1759. https://doi.org/10.1002/hyp.11143.

Brown, S., Lugo, A.E., 1982. The storage and production of organic matter in tropical forests and their role in the global carbon cycle. Biotropica 161–187.

Caflisch, R.E., 1998. Monte carlo and Quasi-Monte Carlo methods. Acta Numerica 7, 1–49.

Candès, E.J., Romberg, J., Tao, T., 2006. Robust uncertainty principles: exact signal reconstruction from highly incomplete frequency information. IEEE Trans. Inf. Theory 52 (2), 489–509.

Chauvel, A., Lucas, Y., Boulet, R., 1987. On the genesis of the soil mantle of the region of Manaus, Central Amazonia, Brazil. Experientia 43 (3), 234–241. https://doi.org/10.1007/BF01945546.

Chen, J., Brissette, F.P., Poulin, A., Leconte, R., 2011. Overall uncertainty study of the hydrological impacts of climate change for a Canadian watershed. Water Resour. Res. 47 (12).

Clark, M.P., Fan, Y., Lawrence, D.M., Adam, J.C., Bolster, D., Gochis, D.J., Hooper, R.P., Kumar, M., Leung, L.R., Mackay, D.S., Maxwell, R.M., Shen, C., Swenson, S.C., Zeng, X., 2015. Improving the representation of hydrologic processes in earth system models. Water Resour. Res. 51 (8), 5929–5956. https://doi.org/10.1002/2015WR017096.

Coe, M.T., Costa, M.H., Howard, E.A., 2008. Simulating the surface waters of the Amazon River basin: Impacts of new river geomorphic and flow parameterizations. Hydrol. Processes 22 (14), 2542–2553.

Collatz, G.J., Ball, J.T., Grivet, C., Berry, J.A., 1991. Physiological and environmental regulation of stomatal conductance, photosynthesis and transpiration - a model that includes a laminar boundary-layer. Agric. Forest Meteorol. 52 (2–4), 107–136.
Cramer, W., Bondeau, A., Schaphoff, S., Lucht, W., Smith, B., Sitch, S., 2004. Tropical forests and the global carbon cycle: impacts of atmospheric carbon dioxide, climate change and rate of deforestation. Philos. Trans. R. Soc. B 359 (1443), 331–343.
Cuartas, L.A., Tomasella, J., Nobre, A.D., Hodnett, M.G., Waterloo, M.J., Múnera, J.C., 2007. Interception water-partitioning dynamics for a pristine rainforest in Central Amazonia: marked differences between normal and dry years. Agric. Forest Meteorol. 145 (1–2), 69–83. https://doi.org/10.1016/j.agrformet.2007.04.008.
Cuartas, L.A., Tomasella, J., Nobre, A.D., Nobre, C.A., Hodnett, M.G., Waterloo, M.J., de Oliveira, S.M., von Randow, R.d.C., Trancoso, R., Ferreira, M., 2012. Distributed hydrological modeling of a micro-scale rainforest watershed in Amazonia: model evaluation and advances in calibration using the new HAND terrain model. J. Hydrol. (Amst) 462–463, 15–27. https://doi.org/10.1016/j.jhydrol.2011.12.047.
da Cruz, P.S., Horne, R.N., Deutsch, C.V., 1999. The quality map: A tool for reservoir uncertainty quantification and decision making. In: SPE Annual Technical Conference and Exhibition. Society of Petroleum Engineers.
Davis, P.J., Rabinowitz, P., 2007. Methods of Numerical Integration. Courier Corporation.
De Rocquigny, E., 2012. Modelling under Risk and Uncertainty: An Introduction to Statistical, Phenomenological and Computational Methods. John Wiley & Sons.
Debusschere, B.J., Sargsyan, K., Najm, H.N., Safta, C., 2017. The Uncertainty Quantification Toolkit (UQTk). Handbook of Uncertainty Quantification.
Detwiler, R.P., Hall, C.A., 1988. Tropical forests and the global carbon cycle. Science 239 (4835), 42–47.
Doostan, A., Owhadi, H., 2011. A non-adapted sparse approximation of PDEs with stochastic inputs. J. Comput. Phys. 230 (8), 3015–3034.
Eldred, M., Burkardt, J., 2009. Comparison of non-intrusive polynomial chaos and stochastic collocation methods for uncertainty quantification. In: 47th AIAA Aerospace Sciences Meeting Including The New Horizons Forum and Aerospace Exposition, p. 976.
Elsheikh, A.H., Hoteit, I., Wheeler, M.F., 2014. Efficient Bayesian inference of subsurface flow models using nested sampling and sparse polynomial chaos surrogates. Comput. Methods Appl. Mech. Eng. 269, 515–537. https://doi.org/10.1016/j.cma.2013.11.001.
Fan, Y., 2015. Groundwater in the Earth's critical zone: relevance to large-scale patterns and processes. Water Resour. Res. 51 (5), 3052–3069.
Fan, Y., Li, H., Miguez-Macho, G., 2013. Global patterns of groundwater table depth. Science 339 (6122), 940–943. https://doi.org/10.1126/science.1229881.
Fan, Y., Miguez-Macho, G., 2010. Potential groundwater contribution to Amazon evapotranspiration. Hydrol. Earth Syst. Sci. 14 (10), 2039–2056. https://doi.org/10.5194/hess-14-2039-2010.
Fang, Y., Leung, L.R., Duan, Z., Wigmosta, M.S., Maxwell, R.M., Chambers, J.Q., Tomasella, J., 2017. Influence of landscape heterogeneity on water available to tropical forests in an Amazonian catchment and implications for modeling drought response: Water Available to Tropical Forest. J. Geophys. Res. 122 (16), 8410–8426. https://doi.org/10.1002/2017JD027066.
Farquhar, G.D., von Caemmerer, S., Berry, J.A., 1980. A biochemical model of photosynthetic CO_2 assimilation in leaves of C-3 species. Planta 149 (1), 78–90.
Fleischbein, K., Wilcke, W., Valarezo, C., Zech, W., Knoblich, K., 2006. Water budgets of three small catchments under montane forest in Ecuador: experimental and modelling approach. Hydrol. Processes 20 (12), 2491–2507.
García, L., Barreiro-Gomez, J., Escobar, E., Téllez, D., Quijano, N., Ocampo-Martínez, C., 2015. Modeling and real-time control of urban drainage systems: a review. Adv. Water Resour. 85, 120–132.
Getirana, A.C.V., Dutra, E., Guimberteau, M., Kam, J., Li, H.-Y., Decharme, B., Zhang, Z., Ducharne, A., Boone, A., Balsamo, G., Rodell, M., Toure, A.M., Xue, Y., Peters-Lidard, C.D., Kumar, S.V., Arsenault, K., Drapeau, G., Ruby Leung, L., Ronchail, J., Sheffield, J., 2014. Water balance in the Amazon Basin from a land surface model ensemble. J. Hydrometeorol. 15 (6), 2586–2614. https://doi.org/10.1175/JHM-D-14-0068.1.
van Genuchten, M.T., 1980. A closed-form equation for predicting the hydraulic conductivity of unsaturated soils. Soil Sci. Soc. Am. J. 44, 892–898.
Ghanem, R.G., Doostan, A., 2006. On the construction and analysis of stochastic models: characterization and propagation of the errors associated with limited data. J. Comput. Phys. 217 (1), 63–81. https://doi.org/10.1016/j.jcp.2006.01.037.
Gilbert, J.M., Jefferson, J.L., Constantine, P.G., Maxwell, R.M., 2016. Global spatial sensitivity of runoff to subsurface permeability using the active subspace method. Adv. Water Resour. 92, 30–42. https://doi.org/10.1016/j.advwatres.2016.03.020.
Gilks, W.R., Richardson, S., Spiegelhalter, D., 1995. Markov Chain Monte Carlo in Practice. CRC Press.
Guan, K., Pan, M., Li, H., Wolf, A., Wu, J., Medvigy, D., Caylor, K.K., Sheffield, J., Wood, E.F., Malhi, Y., Liang, M., Kimball, J.S., Saleska, S.R., Berry, J., Joiner, J., Lyapustin, A.I., 2015. Photosynthetic seasonality of global tropical forests constrained by hydroclimate. Nat. Geosci. 8 (4), 284–289. https://doi.org/10.1038/ngeo2382.
Haario, H., Saksman, E., Tamminen, J., 2001. An adaptive metropolis algorithm. Bernoulli 7 (2), 223–242.
Hall, J., Arheimer, B., Borga, M., Brázdil, R., Claps, P., Kiss, A., Kjeldsen, T.R., Kriauciuniene, J., Kundzewicz, Z.W., Lang, M., 2014. Understanding flood regime changes in Europe: a state of the art assessment. Hydrol. Earth Syst. Sci. 18 (7), 2735–2772.
Hastings, W.K., 1970. Monte Carlo sampling methods using Markov chains and their applications. Biometrika 57 (1), 97–109.
Hillel, D., 1980. Fundamentals of Soil Physics. Academic Press, New York, NY, USA.
Hopp, L., Fatichi, S., Ivanov, V.Y., 2015. Simulating water flow in variably saturated soils: acomparison of a 3-D model with approximation-based formulations. Hydrol. Res. nh2015126. https://doi.org/10.2166/nh.2015.126.
Ivanov, V.Y., Bras, R.L., Vivoni, E.R., 2008. Vegetation-hydrology dynamics in complex terrain of semiarid areas: 1. a mechanistic approach to modeling dynamic feedbacks. Water Resour. Res. 44 (3). https://doi.org/10.1029/2006WR005588.
Ivanov, V.Y., Fatichi, S., Jenerette, G.D., Espeleta, J.F., Troch, P.A., Huxman, T.E., 2010. Hysteresis of soil moisture spatial heterogeneity and the "homogenizing" effect of vegetation. Water Resour. Res. 46 (9), W09521. https://doi.org/10.1029/2009WR008611.
Ivanov, V.Y., Vivoni, E.R., Bras, R.L., Entekhabi, D., 2004. Preserving high-resolution surface and rainfall data in operational-scale basin hydrology: a fully-distributed physically-based approach. J. Hydrol. 298 (1–4), 80–111. https://doi.org/10.1016/j.jhydrol.2004.03.041.
Jarvis, A., Reuter, H.I., Nelson, A., Guevara, E., 2008. Hole-filled SRTM for the Globe Version 4.
Jaynes, E.T., Bretthorst, G.L., 2003. Probability Theory the Logic of Science. Cambridge University Press, Cambridge, UK; New York, NY.
Ji, S., Xue, Y., Carin, L., 2008. Bayesian compressive sensing. IEEE Trans. Signal Process. 56 (6), 2346–2356. https://doi.org/10.1109/TSP.2007.914345.
Karhunen, K., 1946. Zur spektraltheorie stochastischer Prozesse. Ann. Acad. Sci. Fennicae 34.
Kim, C.P., Salvucci, G.D., Entekhabi, D., 1999. Groundwater-surface water interaction and the climatic spatial patterns of hillslope hydrological response. Hydrol. Earth Syst. Sci. Discuss. 3 (3), 375–384.
Kim, J., Dwelle, M.C., Kampf, S.K., Fatichi, S., Ivanov, V.Y., 2016a. On the non-uniqueness of the hydro-geomorphic responses in a zero-order catchment with respect to soil moisture. Adv. Water Resour. 92, 73–89. https://doi.org/10.1016/j.advwatres.2016.03.019.
Kim, J., Ivanov, V.Y., 2015. A holistic, multi-scale dynamic downscaling framework for climate impact assessments and challenges of addressing finer-scale watershed dynamics. J. Hydrol. 522, 645–660. https://doi.org/10.1016/j.jhydrol.2015.01.025.
Kim, J., Ivanov, V.Y., Fatichi, S., 2016b. Environmental stochasticity controls soil erosion variability. Sci. Rep. 6, 22065. https://doi.org/10.1038/srep22065.
Kim, J., Ivanov, V.Y., Fatichi, S., 2016c. Soil erosion assessment—mind the gap. Geophys. Res. Lett. 43 (24), 12,446–12,456. https://doi.org/10.1002/2016GL071480.
Kim, J., Lee, J., Kim, D., Kang, B., 2019. The role of rainfall spatial variability in estimating areal reduction factors. J. Hydrol. 568, 416–426. https://doi.org/10.1016/j.jhydrol.2018.11.014.
Kirchner, J.W., 2009. Catchments as simple dynamical systems: catchment characterization, rainfall-runoff modeling, and doing hydrology backward. Water Resour. Res. 45 (2).
Knio, O.M., Le Maître, O.P., 2006. Uncertainty propagation in CFD using polynomial chaos decomposition. Fluid Dyn. Res. 38 (9), 616–640. https://doi.org/10.1016/j.fluiddyn.2005.12.003.
Kollet, S., Sulis, M., Maxwell, R.M., Paniconi, C., Putti, M., Bertoldi, G., Coon, E.T., Cordano, E., Endrizzi, S., Kikinzon, E., Mouche, E., Mügler, C., Park, Y.-J., Refsgaard, J.C., Stisen, S., Sudicky, E., 2017. The integrated hydrologic model intercomparison project, IH-MIP2: a second set of benchmark results to diagnose integrated hydrology and feedbacks: Integrated Hydrologic Model Intercomparison, IH-MIP2. Water Resour. Res. 53 (1), 867–890. https://doi.org/10.1002/2016WR019191.
Kowalsky, M.B., Finsterle, S., Rubin, Y., 2004. Estimating flow parameter distributions using ground-penetrating radar and hydrological measurements during transient flow in the vadose zone. Adv. Water Resour. 27 (6), 583–599. https://doi.org/10.1016/j.advwatres.2004.03.003.
Krakauer, N.Y., Li, H., Fan, Y., 2014. Groundwater flow across spatial scales: importance for climate modeling. Environ. Res. Lett. 9 (3), 034003. https://doi.org/10.1088/1748-9326/9/3/034003.
Krasnosel'skii, M.A., Pokrovskii, A.V., 1989. Systems with Hysteresis. Springer-Verlag, New York, USA.
Krzysztofowicz, R., 2001. The case for probabilistic forecasting in hydrology. J. Hydrol. 249 (1–4), 2–9.
Le Maître, O.P., Knio, O.M., 2010. Spectral methods for uncertainty quantification. Scientific Computation. Springer Netherlands, Dordrecht.
Leuning, R., 1990. Modelling stomatal behaviour and and photosynthesis of eucalyptus grandis. Funct. Plant Biol. 17 (2), 159–175.
Leuning, R., 1995. A critical appraisal of a combined stomatal - photosynthesis model for C3 plants. Plant, Cell Environ. 18 (4), 339–355. https://doi.org/10.1111/j.1365-3040.1995.tb00370.x.
Lin, G., Karniadakis, G.E., 2009. Sensitivity analysis and stochastic simulations of non-equilibrium plasma flow. Int. J. Numer. Methods Eng. 80 (6–7), 738–766. https://doi.org/10.1002/nme.2582.
Lin, Y.-H., Lo, M.-H., Chou, C., 2015. Potential negative effects of groundwater dynamics on dry season convection in the Amazon River basin. Clim. Dyn. 46 (3–4), 1001–1013. https://doi.org/10.1007/s00382-015-2628-8.
MacKay, D.J., 1998. Introduction to Monte Carlo methods. In: Learning in Graphical Models. Springer, pp. 175–204.
Marelli, S., Sudret, B., 2014. UQLab: A Framework for Uncertainty Quantification in MATLAB. ETH-Zürich.
Marzouk, Y., Xiu, D., 2009. A stochastic collocation approach to Bayesian inference in inverse problems. Commun. Comput. Phys. 6 (4), 826–847. https://doi.org/10.4208/cicp.2009.v6.p826.
Maxwell, R.M., Putti, M., Meyerhoff, S., Delfs, J.-O., Ferguson, I.M., Ivanov, V., Kim, J., Kolditz, O., Kollet, S.J., Kumar, M., Lopez, S., Niu, J., Paniconi, C., Park, Y.-J., Phanikumar, M.S., Shen, C., Sudicky, E.A., Sulis, M., 2014. Surface-subsurface model intercomparison: a first set of benchmark results to diagnose integrated hydrology and feedbacks. Water Resour. Res. 50 (2), 1531–1549. https://doi.org/10.1002/2013WR013725.

McKay, M.D., Beckman, R.J., Conover, W.J., 1979. Comparison of three methods for selecting values of input variables in the analysis of output from a computer code. Technometrics 21 (2), 239–245.
McLaughlin, D., Townley, L.R., 1996. A reassessment of the groundwater inverse problem. Water Resour. Res. 32 (5), 1131–1161.
Miguez-Macho, G., Fan, Y., 2012a. The role of groundwater in the Amazon water cycle: 1. Influence on seasonal streamflow, flooding and wetlands. J. Geophys. Res 117 (D15), D15113. https://doi.org/10.1029/2012JD017539.
Miguez-Macho, G., Fan, Y., 2012b. The role of groundwater in the Amazon water cycle: 2. Influence on seasonal soil moisture and evapotranspiration. J. Geophys. Res. 117 (D15), D15114. https://doi.org/10.1029/2012JD017540.
Miller, K.L., Berg, S.J., Davison, J.H., Sudicky, E.A., Forsyth, P.A., 2018. Efficient uncertainty quantification in fully-integrated surface and subsurface hydrologic simulations. Adv. Water Resour. 111, 381–394. https://doi.org/10.1016/j.advwatres.2017.10.023.
Morss, R.E., Wilhelmi, O.V., Downton, M.W., Gruntfest, E., 2005. Flood risk, uncertainty, and scientific information for decision making: lessons from an interdisciplinary project. Bull. Am. Meteorol. Soc. 86 (11), 1593–1601.
Najm, H.N., 2009. Uncertainty quantification and polynomial chaos techniques in computational fluid dynamics. Annu. Rev. Fluid Mech. 41 (1), 35–52. https://doi.org/10.1146/annurev.fluid.010908.165248.
Neuman, S.P., Fogg, G.E., Jacobson, E.A., 1980. A statistical approach to the inverse problem of aquifer hydrology: 2. Case study. Water Resour. Res. 16 (1), 33–58.
Nobre, A.D., Cuartas, L.A., Hodnett, M., Rennó, C.D., Rodrigues, G., Silveira, A., Waterloo, M., Saleska, S., 2011. Height Above the Nearest Drainage – a hydrologically relevant new terrain model. J. Hydrol. 404 (1–2), 13–29. https://doi.org/10.1016/j.jhydrol.2011.03.051.
Parno, M., Davis, A., Conrad, P., 2014. MIT Uncertainty Quantification (MUQ) Library.
Pokhrel, Y.N., Fan, Y., Miguez-Macho, G., Yeh, P.J.-F., Han, S.-C., 2013. The role of groundwater in the Amazon water cycle: 3. Influence on terrestrial water storage computations and comparison with GRACE. J. Geophys. Res. 118 (8), 3233–3244. https://doi.org/10.1002/jgrd.50335.
Ranzani, G., 1980. Identificação e caracterização de alguns solos da Estação Experimental de Silvicultura Tropical do INPA. Acta Amazon. 10 (1), 7–41.
Razavi, S., Tolson, B.A., Burn, D.H., 2012. Review of surrogate modeling in water resources. Water Resour. Res. 48 (7), W07401. https://doi.org/10.1029/2011WR011527.
Renard, B., Kavetski, D., Kuczera, G., Thyer, M., Franks, S.W., 2010. Understanding predictive uncertainty in hydrologic modeling: the challenge of identifying input and structural errors. Water Resour. Res. 46 (5), W05521. https://doi.org/10.1029/2009WR008328.
Restrepo-Coupe, N., da Rocha, H.R., Hutyra, L.R., da Araujo, A.C., Borma, L.S., Christoffersen, B., Cabral, O.M., de Camargo, P.B., Cardoso, F.L., da Costa, A.C.L., Fitzjarrald, D.R., Goulden, M.L., Kruijt, B., Maia, J.M., Malhi, Y.S., Manzi, A.O., Miller, S.D., Nobre, A.D., von Randow, C., Sá, L.D.A., Sakai, R.K., Tota, J., Wofsy, S.C., Zanchi, F.B., Saleska, S.R., 2013. What drives the seasonality of photosynthesis across the Amazon basin? A cross-site analysis of eddy flux tower measurements from the Brasil flux network. Agric. Forest Meteorol. 182–183, 128–144. https://doi.org/10.1016/j.agrformet.2013.04.031.
Ricciuto, D., Sargsyan, K., Thornton, P., 2018. The impact of parametric uncertainties on biogeochemistry in the E3SM land model: ELM biogeochemical parameter sensitivity. J. Adv. Model. Earth Syst. 10 (2), 297–319. https://doi.org/10.1002/2017MS000962.
Richey, J.E., Ballester, M.V., Davidson, E.A., Johnson, M.S., Krusche, A.V., 2011. Land–Water interactions in the amazon. Biogeochemistry 105 (1–3), 1.
Richey, J.E., Krusche, A.V., Johnson, M.S., Da Cunha, H.B., Ballester, M.V., 2009. The role of rivers in the regional carbon balance. Amazon. Global Change 489–504.
Riley, W.J., Shen, C., 2014. Characterizing coarse-resolution watershed soil moisture heterogeneity using fine-scale simulations. Hydrol. Earth Syst. Sci. Katlenburg-Lindau 18 (7), 2463. https://doi.org/10.5194/hess-18-2463-2014.
Riley, W.J., Subin, Z.M., Lawrence, D.M., Swenson, S.C., Torn, M.S., Meng, L., Mahowald, N.M., Hess, P., 2011. Barriers to predicting changes in global terrestrial methane fluxes: analyses using CLM4Me, a methane biogeochemistry model integrated in CESM. Biogeosciences 8 (7), 1925–1953. https://doi.org/10.5194/bg-8-1925-2011.
Ringeval, B., Houweling, S., van Bodegom, P.M., Spahni, R., van Beek, R., Joos, F., Röckmann, T., 2014. Methane emissions from floodplains in the Amazon Basin: challenges in developing a process-based model for global applications. Biogeosciences 11 (6), 1519–1558. https://doi.org/10.5194/bg-11-1519-2014.
Rudorff, C.M., Melack, J.M., Bates, P.D., 2014. Flooding dynamics on the lower Amazon floodplain: 2. Seasonal and interannual hydrological variability. Water Resour. Res. 50 (1), 635–649. https://doi.org/10.1002/2013WR014714.
Russo, D., Bouton, M., 1992. Statistical analysis of spatial variability in unsaturated flow parameters. Water Resour. Res. 28 (7), 1911–1925. https://doi.org/10.1029/92WR00669.
Saltelli, A., 2002. Making best use of model evaluations to compute sensitivity indices. Comput. Phys. Commun. 145 (2), 280–297.
Salvucci, G.D., Entekhabi, D., 1995. Hillslope and climatic controls on hydrologic fluxes. Water Resour. Res. 31 (7), 1725–1739.
Sargsyan, K., Huan, X., Najm, H. N., 2018. Embedded model error representation for Bayesian model calibration. arXiv:1801.06768.
Sargsyan, K., Najm, H.N., Ghanem, R., 2015. On the statistical calibration of physical models. Int. J. Chem. Kinet. 47 (4), 246–276. https://doi.org/10.1002/kin.20906.
Sargsyan, K., Safta, C., Najm, H.N., Debusschere, B.J., Ricciuto, D., Thornton, P., 2014. Dimensionality reduction for complex models via Bayesian compressive sensing. Int. J. Uncertain. Quantif. 4 (1), 63–93. https://doi.org/10.1615/Int.J.UncertaintyQuantification.2013006821.
Seck, A., Welty, C., Maxwell, R.M., 2015. Spin-up behavior and effects of initial conditions for an integrated hydrologic model. Water Resour. Res. 51 (4), 2188–2210. https://doi.org/10.1002/2014WR016371.
Sivapalan, M., Beven, K., Wood, E.F., 1987. On hydrologic similarity: 2. a scaled model of storm runoff production. Water Resour. Res. 23 (12), 2266–2278.
Smolyak, S.A., 1963. Quadrature and interpolation formulas for tensor products of certain classes of functions. Dokl. Akad. Nauk SSSR 4, 123.
Sobol, I.M., 2001. Global sensitivity indices for nonlinear mathematical models and their Monte Carlo estimates. Math. Comput. Simul. 55 (1–3), 271–280. https://doi.org/10.1016/S0378-4754(00)00270-6.
Sudret, B., 2008. Global sensitivity analysis using polynomial chaos expansions. Reliab. Eng. Syst. Saf. 93 (7), 964–979.
Tarboton, D., 1997. A new method for the determination of flow directions and upslope areas in grid digital elevation models. Water Resour. Res. 33 (2), 309–319.
Thornton, P.E., Lamarque, J.-F., Rosenbloom, N.A., Mahowald, N.M., 2007. Influence of carbon-nitrogen cycle coupling on land model response to CO2 fertilization and climate variability. Global Biogeochem. Cycles 21 (4).
Tibshirani, R., 1996. Regression shrinkage and selection via the lasso. J. R. Stat. Society. Ser. B (Methodol) 267–288.
Tomasella, J., Hodnett, M.G., Cuartas, L.A., Nobre, A.D., Waterloo, M.J., Oliveira, S.M., 2008. The water balance of an amazonian micro-catchment: the effect of interannual variability of rainfall on hydrological behaviour. Hydrol. Processes 22 (13), 2133–2147. https://doi.org/10.1002/hyp.6813.
Tomasella, J., Hodnett, M.G., Rossato, L., 2000. Pedotransfer functions for the estimation of soil water retention in Brazilian soils. Soil Sci. Soc. Am. J. 64 (1), 327–338. https://doi.org/10.2136/sssaj2000.641327x.
Vertessy, R.A., Elsenbeer, H., 1999. Distributed modeling of storm flow generation in an Amazonian rain forest catchment: effects of model parameterization. Water Resour. Res. 35 (7), 2173–2187.
Vidaurre, D., Bielza, C., Larrañaga, P., 2013. A survey of L1 regression. Int. Stat. Rev. 81 (3), 361–387.
Vrugt, J.A., ter Braak, C.J.F., Clark, M.P., Hyman, J.M., Robinson, B.A., 2008. Treatment of input uncertainty in hydrologic modeling: doing hydrology backward with Markov chain Monte Carlo simulation. Water Resour. Res. 44 (12), W00B09. https://doi.org/10.1029/2007WR006720.
Xiu, D., Karniadakis, G.E., 2002. The Wiener–Askey polynomial chaos for stochastic differential equations. SIAM J. Sci. Comput. 24 (2), 619–644. https://doi.org/10.1137/S1064827501387826.
Xiu, D., Tartakovsky, D.M., 2004. Uncertainty quantification for flow in highly heterogeneous porous media. In: Miller, M.W.F.CT., Gray, W.G., Pinder, G.F. (Eds.), Developments in Water Science. In: Part 1 of Computational Methods in Water Resources: Volume 1, 55. Elsevier, pp. 695–703.
Yamazaki, D., Kanae, S., Kim, H., Oki, T., 2011. A physically based description of floodplain inundation dynamics in a global river routing model. Water Resour. Res. 47 (4).
Yeh, W.W.-G., 1986. Review of parameter identification procedures in groundwater hydrology: the inverse problem. Water Resour. Res. 22 (2), 95–108.
Zheng, Z., Dai, H., 2017. Simulation of multi-dimensional random fields by Karhunen–Loève expansion. Comput. Methods Appl. Mech. Eng. 324, 221–247. https://doi.org/10.1016/j.cma.2017.05.022.